UNIVERSITY OF OKLAHOMA

GRADUATE COLLEGE

EFFECT OF CURING TEMPERATURE ON NANOMODIFIED FIBER-REINFORCED POLYMER COMPOSITES

A THESIS

SUBMITTED TO THE GRADUATE FACULTY

In partial fulfillment of the requirements for the

Degree of

MASTER OF SCIENCE

By

ALEXANDRA CHERISE LIEVER
Norman, Oklahoma
2023

Downloaded from SHAREOK. Persistent Handle URL: https://hdl.handle.net/11244/340076

EFFECT OF CURING TEMPERATURE ON NANOMODIFIED
FIBER-REINFORCED POLYMER COMPOSITES

A THESIS APPROVED FOR THE
SCHOOL OF CIVIL ENGINEERING AND ENVIRONMENTAL SCIENCE

BY THE COMMITTEE CONSISTING OF:

Dr. Shreya Vemuganti, Chair

Dr. P. Scott Harvey

Dr. Yingtao Liu

© Copyright by ALEXANDRA C. LIEVER 2023
All Rights Reserved.

This work is dedicated to my parents, Dr. Peter A. Liever and Lisa J. Hughes Liever, whose support never wavered and gave me the courage to pursue my goals. Thank you for always being there for me and making every effort to help those you love to succeed. Your hard work and undeniable tenacity have been an inspiration to me.

Acknowledgements

I would like to express my gratitude to those who have supported me throughout my journey, especially my advisor, Dr. Shreya Vemuganti, as well as my committee members, Dr. P. Scott Harvey, and Dr. Yingtao Liu, without whom this work would not have been possible. I would like to thank my research team, Abdirahman Haibe, Ali Akbarpour, Stephanie Castillo, and Esther Kayondo, as well as those at Fears Structural Laboratory, including John Bullock, Dr. Royce Floyd, Jackson Milner, and Omar Yadak. Additionally, I would like to thank Dr. Chris Billings, Steven Zhao, Jerry Allison, Milad Nourbakhsh, Dr. Joseph Tischler, Mason Rhue, Hesham Aboukeila, Matthew Webb, Dr. Preston Larson, Alyssa Waterson, Charlie Nadal, Dr. Keith Strevett, and Mahaalakshmi Narayanan. Thank you to Transpo Industries, Inc., the Oklahoma Department of Transportation (ODOT), FYFE, the Accelerated Bridge Construction University Transportation Center (ABCUTC), and the OU School of Civil Engineering and Environmental Science (CEES) for making this project possible.

Special thanks to Evan Allison, my sister Robin Liever Ellis, and her husband Ross Ellis, who offered me every encouragement throughout this journey. Thank you for your unshakable faith in me.

Definitions

Terms	Definitions
FRP	Fiber-Reinforced Polymer
CFRP	Carbon Fiber-Reinforced Polymer
CNT	Carbon Nanotube
MWCNT	Multi-walled Carbon Nanotube
SWCNT	Single-walled Carbon Nanotube
VAHT	Vacuum-Assisted Hand Lay-up Technique
SEM	Scanning Electron Microscopy
DSC	Differential Scanning Calorimetry
TGA	Thermogravimetric Analysis
FTIR	Fourier-Transform Infrared

Table of Contents

Chapter 1: Introduction 1

1.1Background 1

1.2Research Objectives, Scope, and Hypotheses 2

1.3Thesis Outline 4

Chapter 2: Review of Literature 5

2.1 Fiber-Reinforced Polymer (FRP) Composites 5

2.2 Use of Carbon Nanotubes (CNTs) in FRP 6

2.3 Curing Kinetics of Epoxy and FRP 8

2.4 Polarity of CNTs and FRP Components 9

2.5 Tensile Behavior of FRP and Impact of Direction of Fiber 10

2.6 Interlaminar Behavior of FRP 11

Chapter 3: Methods and Materials 12

3.1 Testing Overview 12

3.2 CNT Dispersion in Epoxy Resin 13

3.3 Vacuum-Assisted Hand Lay-up Technique (VAHT) for Room Temperature Curing of CFRP Plates 14

3.4 Vacuum-Assisted Hand Lay-up Technique (VAHT) for Oven-Curing of CFRP Plates 16

3.5 Static Tensile Testing of CFRP 18

3.6 Static Tensile Testing of Epoxy Specimens 19

3.7 Peel Testing of CFRP 21

3.8 Scanning Electron Microscopy (SEM) Imaging 24

3.9 Differential Scanning Calorimetry (DSC) 25

3.10 Thermogravimetric Analysis (TGA) 26

Chapter 4: Experimental Results and Discussion 27

4.1 Effect of Nanomodification on CFRP Composites and Epoxy Matrices 27

4.2 Effect of Curing Temperature of CFRP Composites and Epoxy Matrices 36

4.3 CNT Dispersion Quality and SEM 46

4.4 TGA .. 49

4.5 DSC... 50

Chapter 5: Conclusions and Recommendations 55

5.1 Conclusions 55

5.2 Future Work Recommendations 56

References 58

Appendix A: Effect of Freeze-Thaw on Nanomodified Fiber-Reinforced Polymers 61

Introduction to Freeze-thaw 61

Methods and Materials 62

Testing Overview 62

Freeze-thaw Cycling 63

Mechanical Testing 64

Results and Analysis 64

Conclusions for Freeze-thaw Study 68

Future Work with Freeze-thaw 68

References for Freeze-thaw Study 69

Appendix B: Data from CFRP Tensile Testing over Freeze-thaw Cycling 70

List of Tables

Table 1: VAHT Layer Dimensions and Quantities..... 14

Table 2: Results from static tensile testing of CFRP variations cured at different temperatures. 29

Table 3: Results from tension tests done on epoxy cured at room temperature. 31

Table 4: Results from tension tests done on CFRP cured at room temperature. 33

Table 5: Results from peel tests done on CFRP cured at room temperature. 36

Table 6: Results from static tension tests on nanomodified epoxy cured at room temperature (RT, 30˚C) and oven temperature (Oven, 110 ˚C). 38

Table 7: Percent increase of mechanical properties of epoxy with respect to respective CNT types when cured at 110 ˚C instead of 30 ˚C. 38

Table 8: Results from static tension tests on nanomodified CFRP cured at room temperature (RT, 30˚C) and oven temperature (Oven, 110 ˚C). 42

Table 9: Percent increase of mechanical properties of CFRP with respect to respective CNT types when cured at 110 ˚C instead of 30 ˚C. 42

Table 10: Results from peel tests on nanomodified CFRP cured at room temperature (RT, 30˚C) and oven temperature (Oven, 110 ˚C)..... 44

Table 11: Percent increase of interfacial adhesion strength of CFRP with respect to respective CNT types when cured at 110 ˚C instead of 30 ˚C. 46

Table 12: Onset and end of weight loss from TGA for all epoxy types. 50

Table 13: DSC results for all cured epoxy and CFRP types cured at room temperature (RT, 30 ˚C) and cured in the oven (110 ˚C). 54

Table 14: Results from tensile testing of CFRP after zero freeze-thaw cycles. 70

Table 15: Results from tensile testing of CFRP after 50 freeze-thaw cycles. 71

Table 16: Results from tensile testing of CFRP after 100 freeze-thaw cycles. 72

Table 17: Results from tensile testing of CFRP after 150 freeze-thaw cycles. 73

Table 18: Results from tensile testing of CFRP after 200 freeze-thaw cycles. 74

Table 19: Results from tensile testing of CFRP after 250 freeze-thaw cycles. 75

List of Figures

Figure 1: Examples of CFRP used to wrap damaged (a) beams; (b) columns. (Alkhrdaji 2015) .. 1

Figure 2: CNT Manufacturing Process (Filchakova 2021)..... 6

Figure 3: Schematic of off-axis versus on-axis loading: (a) Off-axis fiber orientation; (b) On-axis Fiber Orientation (c) Off-axis failure mode in tension, loaded at 0°; (d) On-axis failure mode in tension, loaded at 0°. 10

Figure 4: Specimen matrix for epoxy resin, CFRP tensile, and peel specimens determined after initial testing..... 12

Figure 5: CNT Dispersion Equipment. 13

Figure 6: VAHT setup (a) Schematic of CFRP plate layers; (b) VAHT lab setup with vacuum pump; (c) Rolling epoxy into carbon fiber textile. 15

Figure 7: Oven curing (a) CFRP plate in vacuum bag; (b) Bagged CFRP plate in lab oven. 17

Figure 8: Tensile testing setup (a) Instron 5967 Universal Testing Frame tensile grips with specimen loaded; (b) Instron AVE 2 Non-Contacting Video Extensometer with tensile test setup; (c) CFRP tabbed tensile specimen. 19

Figure 9: Epoxy tensile testing setup (a) Epoxy specimen loaded into tensile grips; (b) Epoxy specimen for tensile testing. 20

Figure 10: Steps for manufacturing CFRP composite for peel testing. 21

Figure 11: (a) Peel specimen in oven for curing; (b) Prepared peel specimen. 22

Figure 12: Peel specimen set up for testing. 24

Figure 13: Differential Scanning Calorimeter 25

Figure 14: TGA Equipment: (a) TGA machine; (b) Sample pan and chamber. 26

Figure 15: Average tensile strength of CFRP types (neat-N, pristine CNT-P, and functionalized-COOH – F). 28

Figure 16: Mean (a) Tensile strength, (b) Strain at failure, (c) Young's Modulus, (d) Median stress-strain relationship of neat, pristine 1%, and functionalized 1% epoxy cured at room temperature. 30

Figure 17: Representative neat (top) and nanomodified (bottom) epoxy resin specimens after tensile testing. 31

Figure 18: Mean (a) tensile strength, (b) strain at failure, (c) Young's modulus, and (d) median stress-strain relationship of neat, pristine 1%, and functionalized 1% CFRP cured at room temperature. 33

Figure 19: (a) Representative CFRP tensile specimen after failure; (b) Failure mode of CFRP tensile specimen. 34

Figure 20: (a) Stress-strain relationship, (b) mean interfacial adhesion strength, (c) peel interface, (d) specimen during testing, and (e) specimen after failure for neat, pristine 1%, and functionalized 1% CFRP cured at room temperature. 35

Figure 21: Stress-strain relationship for (a) neat epoxy, (b) pristine CNT epoxy (1% wt. of epoxy), and (c) functionalized-COOH CNT epoxy (1% wt. of epoxy) cured at room temperature (30 °C) and elevated oven temperature (110 °C). 37

Figure 22: Mean (a) tensile strength, (b) strain at failure, and (c)Young's Modulus of epoxy resin cured at room temperature (30 ℃) and elevated temperature (110 ℃)..... 40

Figure 23: Stress-strain relationship for median (a) neat CFRP, (b) pristine CNT CFRP (1% wt. of epoxy), and (c) functionalized-COOH CNT CFRP (1% wt. of epoxy) cured at room temperature (30 °C) and elevated oven temperature (110 °C). 41

Figure 24: Mean (a) tensile strength, (b) strain at failure, and (c)Young's modulus of CFRP cured at room temperature (30 ℃) and elevated temperature (110 ℃)..... 43

Figure 25: (a) Load-crosshead displacement relationship and (b) mean interfacial adhesion strength for CFRP cured at room temperature (30 ˚C) and elevated temperature (110 ˚C). 45

Figure 26: SEM images of (a) neat 25K X, (b) neat 50K X, (c) pristine CNT 5K X, (d) pristine CNT 25K X, (e) pristine CNT 25K X, (f) functionalized-COOH CNT 25K X, (g) functionalized-COOH CNT 25K X, (h) functionalized-COOH CNT 50K X epoxy cured at room temperature. 49

Figure 27: TGA results for all epoxy types. 49

Figure 28: DSC curves for dynamic testing of (a) neat, (b)P 1%, (c) and F 1% epoxy and CFRP cured at room temperature (RT 30 ˚C) and elevated temperature (Oven 110 ˚C). 53

Figure 29: Matrix of CFRP types manufactured for freeze-thaw cycling. 63

Figure 30: Freeze-thaw cycling in environmental chamber. 64

Figure 31: Evolution of (a) strength, (b) strain, and (c) modulus of elasticity of CFRP tensile specimens over 250 freeze-thaw cycles. 66

Figure 32: Stress-strain relationship for CFRP after (a) 0 freeze-thaw cycles and (b) 250 freeze-thaw cycles. 67

Abstract

Dispersion of pristine and functionalized-COOH carbon nanotubes (CNTs) into the resin matrix used to develop fiber-reinforced polymer (FRP) composites is known to improve FRP properties such as shear strength, UV resistance, strength, and stiffness. Nanomodification of the FRP matrix with CNTs is also known to improve bonds within the FRP. However, there is still a gap in knowledge on the effect of temperature on curing characteristics when CNTs are incorporated. In this study, mechanical testing and material characterization of nanomodified FRP composites was conducted to identify the effects of curing under room temperature (30 °C) and elevated temperature (110 °C). The resin for FRP composites was nanomodified with pristine and functionalized multi-walled carbon nanotubes using a standard dispersion protocol. FRP composites were fabricated using vacuum assisted hand layup techniques and prepared for ASTM standard testing. Static tensile testing and interfacial adhesion tests were conducted to evaluate the mechanical performance. Differential scanning calorimetry and thermogravimetric analysis were performed to determine curing characteristics to inform on the polymerization of nanomodified resins cured under the two temperature conditions. Scanning electron microscopy was performed to identify CNT dispersion characteristics. It was found that curing FRP composites with nanomodified resins at elevated temperatures increased the tensile and interfacial adhesion strength and stiffness and also reduced ductility. It can be understood from this study how target performance metrics in a wide range of structural applications can be achieved in FRP composites by incorporating nanomodified resins cured at varying temperatures.

Chapter 1: Introduction

1.1 Background

Fiber-reinforced polymer (FRP) composites have become a popular material in applications that require a high strength-to-weight ratio, superior thermal and mechanical properties, and corrosion resistance (Uddin 2013). FRP composites can be made into bars, plates, wraps (shown in Figure 1), and other elements that are implemented into a structural system (Alkhrdaji 2015). In the field of civil engineering, FRP has been successfully implemented in repair and strengthening of deteriorating buildings and bridges, as well as new construction. The rapid curing time of FRP on-site and its ability to be pre-cast and even 3D-printed into different shapes has proved to be extremely useful in civil engineering applications. In order to further improve properties of FRP for structural application, research has previously been done on the addition of carbon nanotubes (CNTs) to the FRP matrix (i.e., nanomodification) (Boroujeni et al. 2014). CNTs have been extremely popular in the scientific community due to their excellent strength, thermal properties, and electrical properties. The dispersion of CNTs into the FRP matrix

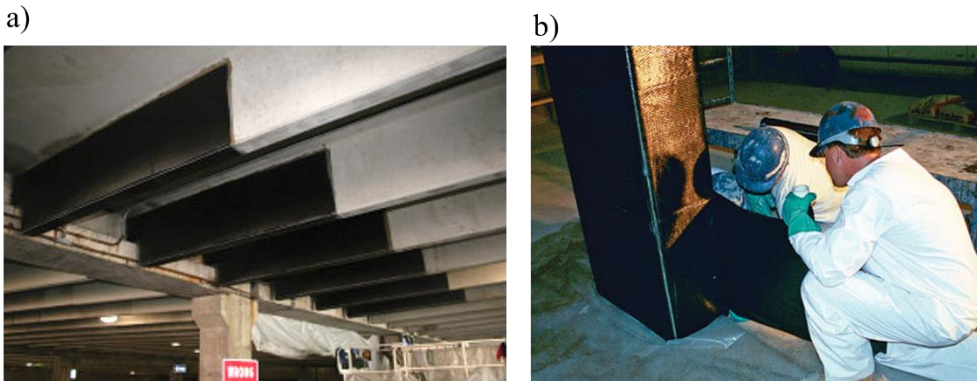

Figure 1: Examples of CFRP used to wrap damaged (a) beams; (b) columns. (Alkhrdaji 2015)

has been shown to improve many properties of composites, such as thermal resistance, durability against weathering and cracks, strength, and stiffness. These improvements in properties are largely due to the enhancement of the interlaminar bonding in the FRP composite (Li et al. 2021).

However, the addition of CNTs into the epoxy matrix may affect the mechanical and material properties of the FRP composite, and investigation is required to understand how CNTs affect cured FRP products. In this study, CNTs functionalized with a carboxyl (COOH) group, as well as pristine CNTs were explored as a dispersant in the FRP epoxy matrix to explore the effect of different CNT types on FRP composites. Additionally, there is a gap in knowledge on how curing of FRP is affected by nanomodification. Curing is a driving factor in the performance of the polymer and resulting FRP composite. While significant research has been done on the effect of curing temperature on FRP composites without nanomodification, the effect of the CNTs on curing is not as clear (Singh et al. 2018). Therefore, the effect of curing temperature on the properties of nanomodified carbon fiber-reinforced polymer (CFRP) composite is investigated in this study. By accounting for the effect of this curing parameter, target performance metrics in a wide range of structural applications can be achieved in FRP composites by incorporating nanomodified resins cured at varying temperatures.

1.2 Research Objectives, Scope, and Hypotheses

The following are objectives of this research project:

- Evaluate the changes in mechanical and material properties of a CFRP composite nanomodified with 1% wt. pristine and 1% wt. functionalized-COOH CNTs cured at room temperature (30 °C) and elevated temperature (110 °C).

- Determine interfacial adhesion of CFRP nanomodified with 1% wt. pristine and 1% wt. functionalized-COOH CNT cured at room temperature (30 ℃) and elevated temperature (110 ℃).
- Determine the tensile behavior of epoxy modified with 1% wt. pristine and 1% wt. functionalized-COOH CNTs cured at room temperature (30 ℃) and elevated temperature (110 ℃).
- Evaluate the material characteristics of CFRP nanomodified with 1% wt. pristine and 1% wt. functionalized-COOH CNTs room temperature (30 ℃) and elevated temperature (110 ℃) through scanning electron microscopy, thermogravimetric analysis, and differential scanning calorimetry.

Results from testing will reveal differences in behavior between different variations of the FRP matrix which indicate how curing procedure and nanomodification interact and can be adjusted to achieve different levels of performance depending on the desired application.

The following hypotheses are proposed for this research:

i. Dispersion of pristine or functionalized-COOH CNTs in the CFRP matrix may increase the tensile strength and interfacial adhesion of the CFRP cured at both room temperature (30 ℃) and elevated temperature (110 ℃).
ii. CFRP with functionalized-COOH CNTs may display higher strength compared to FRP with pristine CNTs due to enhanced ability to disperse in the epoxy matrix.

iii. Increasing the curing temperature of the epoxy matrix used in CFRP from room temperature (30 °C) to 110 °C may result in a stronger, more brittle matrix due to changes in polymerization.

iv. Dispersal of CNTs in the epoxy matrix may increase the energy threshold necessary for the epoxy to cure adequately. Therefore, additional energy may be necessary for nanomodified composites to cure.

1.3 Thesis Outline

This thesis includes five chapters and two appendices. Chapter 1 introduces the topic and motivation for this work and outlines the main objectives. Chapter 2 is a review of existing literature that is relevant to FRP composites, CNTs, epoxies, and the interaction between these three materials. Chapter 3 contains information regarding all testing and material manufacturing methods used in this study. Chapter 4 consists of experimental results and discussion of results. Chapter 5 discusses conclusions and recommendations based on results. Preliminary investigation for a path towards future work is also discussed. Appendix A contains a supplemental study on the effects of freeze-thaw on FRP. In Appendix B, data from tensile testing of CFRP for investigation of freeze-thaw effects is presented.

Chapter 2: Review of Literature

2.1 Fiber-Reinforced Polymer (FRP) Composites

A composite material is a combination of two or more materials that form a new cohesive material with more desirable properties than the original materials (Jain et al. 2012). FRP composites consist of directional fibers and a matrix that provides load transfer between the fibers and keeps them in the desired orientation (Uddin 2013). Common matrix materials include polymer-based resins and epoxies, while common synthetic fibers are carbon (CFRP), glass (GFRP), and aramid (AFRP) (Jain et al. 2012, Uddin 2013). Each type of fiber has its own mechanical properties and costs, which are evaluated for every application. In the construction industry, thermoset polymer matrices in FRP composites are more prevalent because the bonds permanently crosslink within the polymer, making the composite durable with high thermal stability (Cividanes et al. 2017). FRP has gained popularity in the construction industry over the last decades, in part because of its inherent high strength-to-weight ratio, high specific stiffness, corrosion resistance, and environmental durability (Uddin 2013). Because of its environmental durability, less maintenance and need for replacement, FRP could lead to longer life spans for structures reinforced with FRP. Additionally, FRP is commonly used for infrastructure retrofitting and strengthening because of its short casting times and ability to form around almost any shape (Jain et al. 2012). FRP can be manufactured in many ways, including pultrusion into bars, casting as a plate or directly onto a member, or injecting into molds (Jain et al. 2012). These mechanical characteristics and versatility in manufacturing methods make FRP a suitable choice for long-term applications on new or retrofitted buildings, bridges, and other structures.

2.2 Use of Carbon Nanotubes (CNTs) in FRP

CNTs are rolled-up sheets of carbon (graphene) that form cylindrical tubes as shown in Figure 2. CNTs with several layers of these cylindrical layers, called multi-walled carbon nanotubes (MWCNTs), can utilize different stacking alignments of the carbon lattice, enhancing stiffness and structural integrity (Li et al. 2021). CNTs have extremely high strength-to-weight ratios compared to materials like steel. The dispersion of CNTs into the FRP matrix (i.e., nanomodification) has been shown to improve many properties of the composite, such as thermal resistance, durability against weathering and cracks, strength, and stiffness (Li et al. 2021).

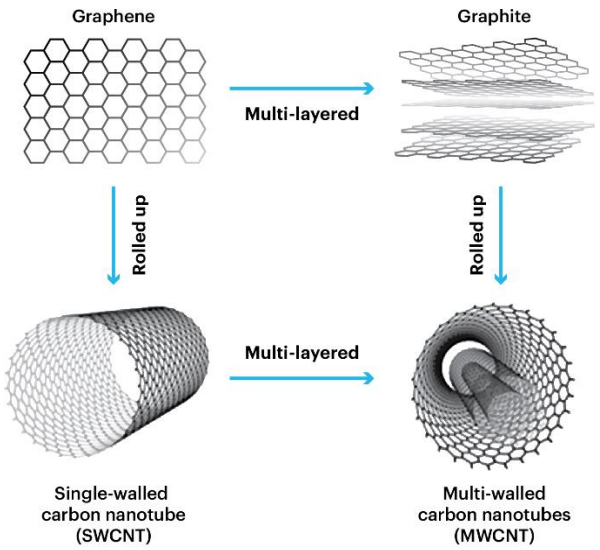

Figure 2: CNT Manufacturing Process (Filchakova 2021).

These improvements in properties are due largely to the enhancement of the interlaminar bonding of the FRP composite (Li et al. 2021). A study done in 2016 revealed that mechanical performance of concrete reinforced with FRP was greatly enhanced by the addition of CNTs to the FRP matrix (Irshidat et al. 2016). The CNTs bridge the gaps formed by cracks and hold laminations together that might otherwise peel apart (Chen et al. 2003). Overall, nanomodification of the FRP matrix improves bonds within the FRP, allowing more engagement with the reinforced structural member, increasing the FRP composite's contribution to member strengthening before failing along a lamination interface.

There are some challenges associated with the uniform dispersion of CNTs in epoxy matrices. Without proper dispersal of the CNTs in the matrix and in the final FRP product, the performance of the composite will suffer (Cividanes et al. 2017). Reasons for CNT agglomeration includes their hydrophobic nature and high aspect ratio. Because of their high aspect ratio, they are easily tangled (Chakraborty et al. 2011). Another reason for CNT agglomeration is strong intermolecular van der Waals forces of the CNT. Ultrasonication is a method commonly used to break these bonds (Soliman et al. 2012) and was used in this study during the dispersion process.

Improvement of mechanical properties of nanomodified composites depends heavily on the ability of the CNT to bond with the epoxy matrix, thus engaging it. If the CNTs are not bonded to the matrix, they act as cavities in the epoxy matrix, weakening it. Therefore, CNTs must be properly bonded to the epoxy matrix to enhance the composite. To increase the affinity between the CNT and epoxy matrix, CNTs can be functionalized with different chemical groups, changing how they interact in solvents. MWCNTs chemically functionalized with a carboxyl group (COOH) are popular among researchers for their ability to enhance dispersion quality and increase interfacial adhesion between the CNT and epoxy (Zhang et al. 2019). The attraction between epoxy and functionalized-COOH CNT is stronger than the intermolecular forces between CNTs that keep them agglomerated. Therefore, the CNTs can break away from each other and bond with the epoxy in a stable manner (Cividanes et al. 2014). A study at the Beijing University of Chemical Technology revealed that the addition of carboxyl groups (COOH) to CNTs resulted in a 59% increase in flexural strength of an FRP composite. The COOH groups attached to the CNT create more bonds between the CNT and epoxy. Pristine, or unmodified, CNTs are not expected to have as strong a bond with the epoxy, leading to lower dispersion quality and less contribution to the

composite (Cividanes et al. 2014). In this study, multi-walled COOH-functionalized CNTs were utilized along with the multi-walled pristine (unmodified) CNTs.

2.3 Curing Kinetics of Epoxy and FRP

Isothermal and dynamic DSC methods have been used to prove the changes in curing kinetics when CNTs are dispersed in epoxy. Previous studies on Bisphenol-F resin, which is similar to Bisphenol-A resin used in this study, have shown that there is an increase of total heat in the epoxy curing reaction when modified with a high concentration of carbon nanofillers, as well as a period of accelerated curing in the early stages of the curing process (Allaoui et al. 2009, Zhou et al. 2009). It is suggested that carbon nanomaterials act as catalysts that begin the curing reaction sooner than neat epoxy. However, later in the curing process, the curing rate slows, as the viscosity of the epoxy is too high for hardener to reach molecules that have not yet reacted, leading to a different degree of cure. Other studies reported no significant changes in total energy during the reaction, as well as indicators of CNTs hindering the curing (Allaoui et al. 2009). Another study found that the addition of functionalized-COOH MWCNTs to a Bisphenol-A resin increased the activation energy required for the epoxy to cure (Abdalla et al. 2008). Therefore, additional energy beyond the standard reaction is necessary in this case to reach an adequate degree of cure.

Further, researchers have found that addition of MWCNTs lower the glass transition temperature (T_g) of the epoxy, preventing vitrification of the polymer. T_g indicates the amount of energy that the polymer chains need to break out of their structure. If the T_g is low, not much energy is required, and the polymer stays more pliable with a less rigid structure (Polymer Science Learning Center 2023). During the polymer curing reaction, when the vitrification point is reached,

the polymer transitions from a rubbery material to a glass-like material, leading to reduced mobility of the reactants. If vitrification occurs early in the curing reaction, the degree of cure for the epoxy will be lower, as not all reactants have been able to interact yet (Dodiuk et al. 2022). Therefore, without adding additional energy to the curing polymer, the neat epoxy will likely reach a point of vitrification sooner than the nanomodified version.

2.4 Polarity of CNTs and FRP Components

Several environmental effects on epoxy curing were considered to eliminate factors that may weaken the FRP lamination. Particularly, the effect that solvent polarity has on the ability of CNTs to disperse properly was of interest. Rajendran found that the attraction between functionalized-COOH CNTs and a solvent was significantly affected by the polarity of the solvent, where high-polarity solvents created a high degree of affinity between the functionalized-COOH CNT and solvent. However, the same is not true for pristine CNTs that act as nonpolar molecules (Rajendran et al. 2022). The addition of the hydroxyl group in functionalized-COOH CNTs increases the electronegativity of the CNT, creating a more polar molecule. The polar-polar affinity between the solvent and CNT enables the CNTs to disperse in the solvent with less energy compared to a non-polar solvent, which would behave similarly to oil and water (Rajendran et al. 2022). The epoxy used in this study was Bisphenol-A based, with this variation often abbreviated in literature as DGEBA (diglycidyl ether of Bisphenol-A), a low polarity molecule. However, a significant number of researchers have utilized Bisphenol-A and Bisphenol-F epoxies, resulting in successful CNT dispersions with improved mechanical properties in composites and epoxies (Mansoor et al. 2014, Bansal et al. 2022). Therefore, the low polarity of the Bisphenol-A base was determined to be a nonlimiting factor in this case.

2.5 Tensile Behavior of FRP and Impact of Direction of Fiber

Since interlaminar bonding of the epoxy between fibers is a critical property that controls much of the FRP composite behavior, this study focused on revealing the interlaminar response of the FRP controlled in large part by the epoxy matrix. Testing of the biaxial FRP at a 45° angle from the direction of loading (i.e., off-axis, Figure 3(a)) is a more effective method than loading at 0° (i.e., on-axis, Figure 3(b)) to reveal the response of the epoxy matrix in the FRP (Soliman et al. 2012). By testing the fibers in their "weak" axis with less resistance to deformation, the epoxy matrix is forced to engage more to sustain loading, and specimens ultimately fail in fiber pullout (Figure 3(c)) instead of fiber fracture (Figure 3(d)). Because interlaminar bond strength of the FRP relies significantly on the matrix properties, this method of testing is an effective way to monitor the differences that nanomodification of the epoxy matrix present.

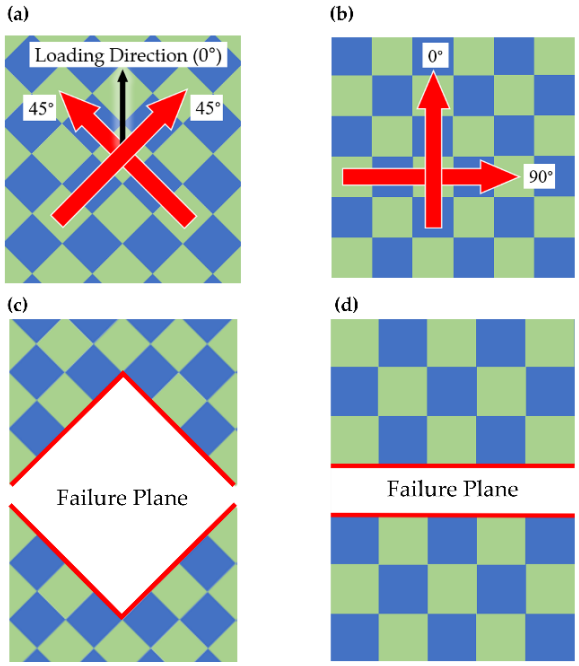

Figure 3: Schematic of off-axis versus on-axis loading: (a) Off-axis fiber orientation; (b) On-axis Fiber Orientation (c) Off-axis failure mode in tension, loaded at 0°; (d) On-axis failure mode in tension, loaded at 0°.

2.6 Interlaminar Behavior of FRP

While FRP has many beneficial mechanical properties that make it a strong and durable material, it is limited by the bond between laminations of the composite. Materials that are manufactured in laminations are prone to crack propagation and interlaminar failure (Khan et al. 2011). Since there is a defined plane of the material that is weaker than the rest, the material will tend to fail in that path. Therefore, it is critical to investigate the interfacial adhesion along the laminate faces of an FRP composite. Previous studies show that interfacial adhesion can improve with the addition of CNTs to a composite. This effect is credited to the interlocking of the CNTs with the epoxy matrix, which effectively bridges smaller cracks and slowing crack progression (Khan et al. 2011, Joshi et al. 2012).

Chapter 3: Methods and Materials

3.1 Testing Overview

Seven types of CFRP plates were cast initially: neat (no nanotubes), nanomodified with pristine MWCNTs (0.5%, 1.0%, and 1.5% by weight pristine nanotubes), and nanomodified with functionalized MWCNTs (0.5%, 1.0%, 1.5% wt. functionalized-COOH nanotubes). After initial static tensile testing, it was determined that the epoxy and CFRP configurations that warranted further investigation through this project were neat, 1% weight functionalized-COOH MWCNTs, which had the highest tensile strength, and 1% weight pristine MWCNTs, to compare with functionalized-COOH results. Testing conducted with these three types includes static tensile testing of epoxy and CFRP composites, as well as peel testing of CFRP. Each of these tests were performed on room temperature cured (30°C (86 °F)) and oven cured (110°C (230 °F)) specimens of respective types. 110 ℃ curing temperature was selected to match the epoxy manufacturer's selected curing temperature used when they tested for the characteristic epoxy properties.

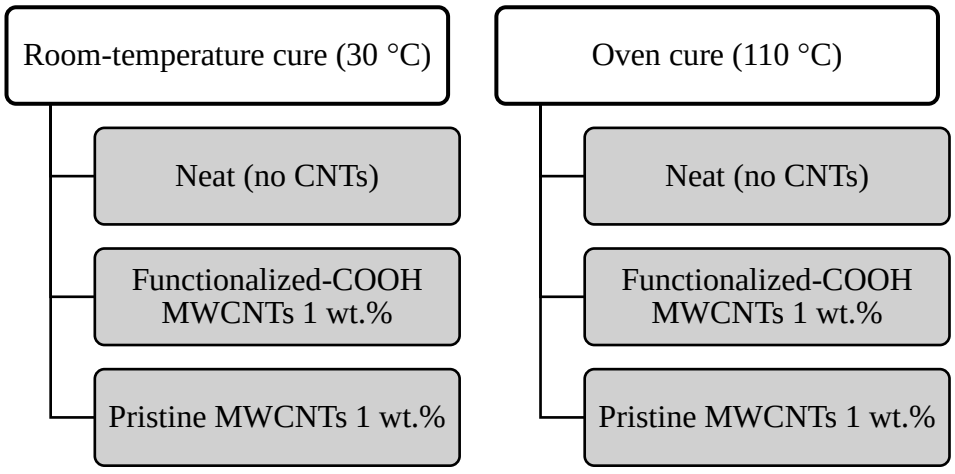

Figure 4: Specimen matrix for epoxy resin, CFRP tensile, and peel specimens determined after initial testing.

Additional material investigations of the epoxy, including SEM imaging, DSC, and TGA were conducted to understand the baseline characteristics of the materials, as well as changes due to curing temperature.

3.2 CNT Dispersion in Epoxy Resin

MWCNTs were dispersed in low viscosity 635 Thin Epoxy Resin from US Composites. The procedure was identical for functionalized and pristine nanotubes. The MWCNTs were from Cheap Tubes, Inc., with a 20-30 nm outer diameter, 5-10 nm inner diameter, and 10-30 µm length. All handling of unsuspended CNTs was under a fume hood to avoid airborne CNT contamination. The amount of CNTs added to the epoxy was based on weight percentage of the epoxy. The CNT-epoxy mixture was mechanically stirred by hand for approximately 30 seconds. The beaker was then covered with a glass plate and placed in an ultrasonic water bath (Branson 1800) at 40 kHz and degassed for five minutes. The setting was then switched to sonic with a bath temperature of 40 °C (104 °F) for one hour. The beaker was then stirred on an 80 °C (176 °F) magnetic stirrer (Four E's Scientific 5-inch) with a 2-inch magnetic bar at 800 rpm for two hours. After stirring,

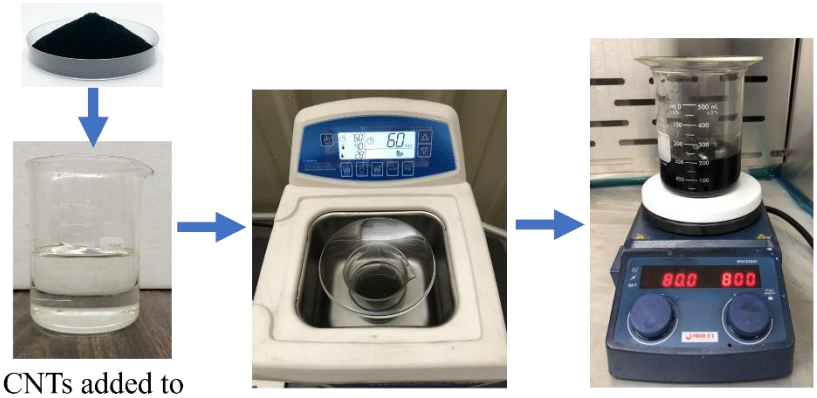

Figure 5: CNT Dispersion Equipment.

the epoxy resin was left to cool to room temperature, approximately 30 °C (86 °F) before adding any hardener.

3.3 Vacuum-Assisted Hand Lay-up Technique (VAHT) for Room Temperature Curing of CFRP Plates

All CFRP composite laminates for tensile specimens were cast using the vacuum-assisted hand lay-up technique (VAHT) in compliance with ASTM D5687. Before casting a nanomodified CFRP plate, nanotubes were already dispersed in the thin epoxy resin and cooled to room temperature. A 61 cm by 61 cm flat steel plate was secured to a stable and level surface as a base layer. Table 1 specifies materials sourced from US Composites that were cut to size to cast a 50.8 cm by 50.8 cm plate of CFRP.

Table 1: VAHT Layer Dimensions and Quantities

Material	**Size of Layer**	**Quantity of Layers**
Nylon Release Film	58 cm by 58 cm	2
Breather Cloth	53 cm by 53 cm	1
Perforated Release Film	53 cm by 53 cm	1
Peel Ply	53 cm by 53 cm	2
Biaxial Plain Weave Carbon Fiber Textile	50.8 cm by 50.8 cm	6 for Tensile Specimens 4 for Specimen Tabs

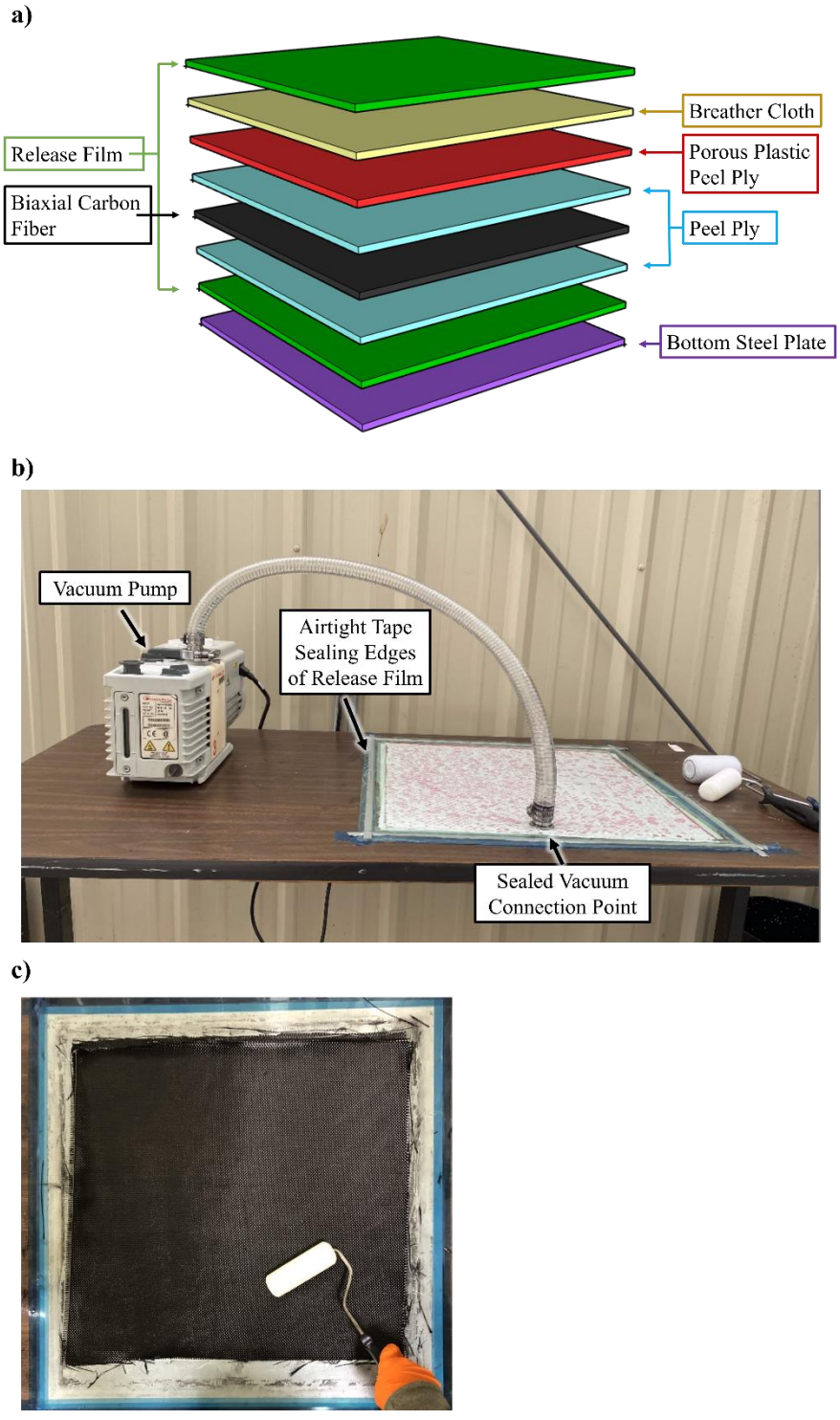

Figure 6: VAHT setup (a) Schematic of CFRP plate layers; (b) VAHT lab setup with vacuum pump; (c) Rolling epoxy into carbon fiber textile.

The previously nanomodified (or neat for control specimens) epoxy resin is mixed into epoxy hardener (556 2:1 Slow Epoxy Hardener) in a 2:1 ratio. The mixture was stirred by hand with a non-absorbent utensil for 30 seconds, or until mix was homogeneous. The materials were placed in the order depicted in Figure 6(a). The carbon fiber textile was placed with fiber weave aligned at 0° and 90°, as shown in Figure 3(b). A dense foam roller was used to fully saturate the material layers by spreading and rolling the epoxy in between each peel ply and carbon fiber layer. The remaining layers were not rolled. Airtight tape was applied to the edges of the steel plate and the release film was placed on top by pressing the edges firmly on the tape to seal the edges. Failure to fully saturate the materials with the epoxy will result in damage to the composite's mechanical properties. To avoid oversaturation, which also hinders performance, a vacuum pump (Edwards, 1.5×10^{-3} Torr) was attached just beneath the top release film layer to create suction that will pull the epoxy towards the breather cloth, which absorbed any excess epoxy. The VAHT setup is shown in Figure 6(b). For room-temperature curing, the approximate temperature of the laboratory was 30 °C throughout the casting process. The vacuum pump remained running for six hours and was then turned off. The FRP plate was left in place for 24 hours. After 24 hours, all layers were peeled from the carbon fiber plate and the plate was left at room temperature to cure for an additional 24 hours. The outside 25.4 mm perimeter of the plate, as well as the immediate area where the vacuum hose was placed, was not used for specimens to avoid material inconsistencies.

3.4 Vacuum-Assisted Hand Lay-up Technique (VAHT) for Oven-Curing of CFRP Plates

To cast oven cured CFRP, the wet lay-up procedure was performed at room temperature, approximately 30 °C. However, the lay-up of textiles was removed from the steel plate and placed

into a vacuum bag (Polyamide and Polyethylene, Hibag brand) immediately after all layers were added. Flat CFRP plates were placed on the top and bottom of the textile lay-up to prevent warping in the oven since the steel plate was not transferable. The bag was sealed, and the vacuum pump was connected to the vacuum connection point built into the bag. The vacuum pump was run for three minutes, until epoxy began to show in the breather cloth layer. The vacuum was then disconnected, and the bag valve was sealed to maintain the vacuum. The bag was placed on a flat rack in a convection lab oven (Quincy Lab, Inc.) pre-heated to 110 °C and left for 12 hours. After

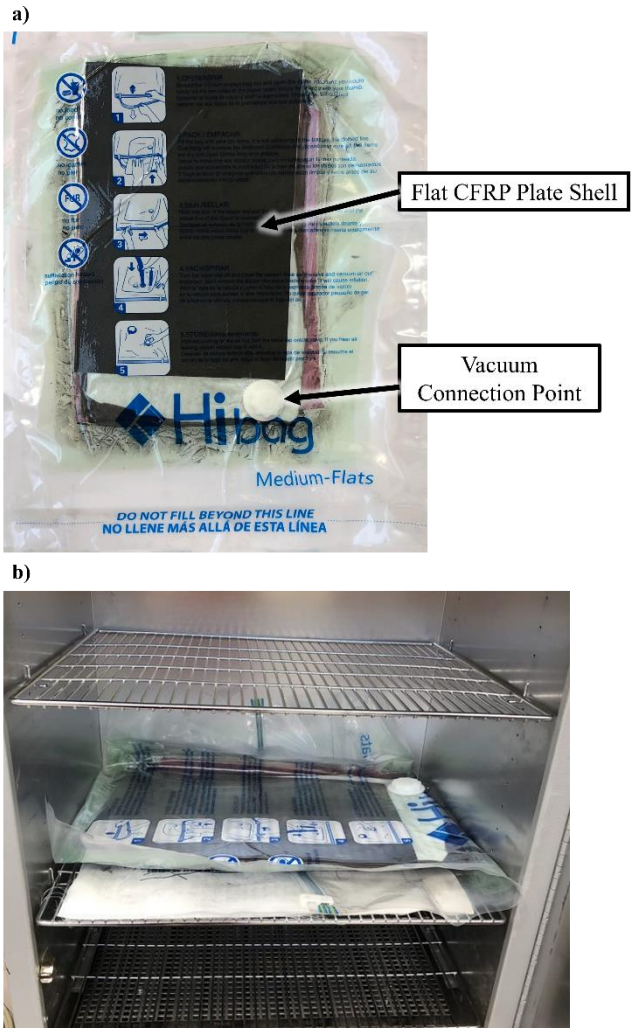

Figure 7: Oven curing (a) CFRP plate in vacuum bag; (b) Bagged CFRP plate in lab oven.

12 hours, the bag was removed from the oven and laid on a flat surface for 36 hours. The composite plate was then removed from the vacuum bag to be cut into specimens.

3.5 Static Tensile Testing of CFRP

Static tensile testing was done in compliance with ASTM D3039-17. All tensile testing was performed on an Instron 5967 Universal Testing Frame with an Instron AVE 2 Non-Contacting Video Extensometer. Tensile specimens were 127 mm by 15 mm. 18 mm by 15 mm tabs for the tensile specimens were four-layer off-axis carbon fiber cast with VAHT at the same curing temperature of the respective specimen and adhered to specimens with high-viscosity TYFO Saturant Epoxy (FYFE Co.). Flat-faced clamps were placed over the tabs for 48 hours at room temperature for curing. A gauge length of 50.8 mm was marked for all specimens with a white paint marker to create a high-contrast image for the video extensometer. Specimens were aligned with the direction of loading, and grips were tightened approximately 3 mm away from the edge of the specimen tabs. Testing of five specimens per type was done at a displacement rate of 1 mm per minute until failure. Ultimate tensile strength was calculated per ASTM D3039 Equation 5.

$$F^{tu} = P^{max}/A \tag{3.1}$$

Where:

F^{tu} = ultimate tensile strength

P^{max} = maximum force before failure

A = Average cross-sectional area

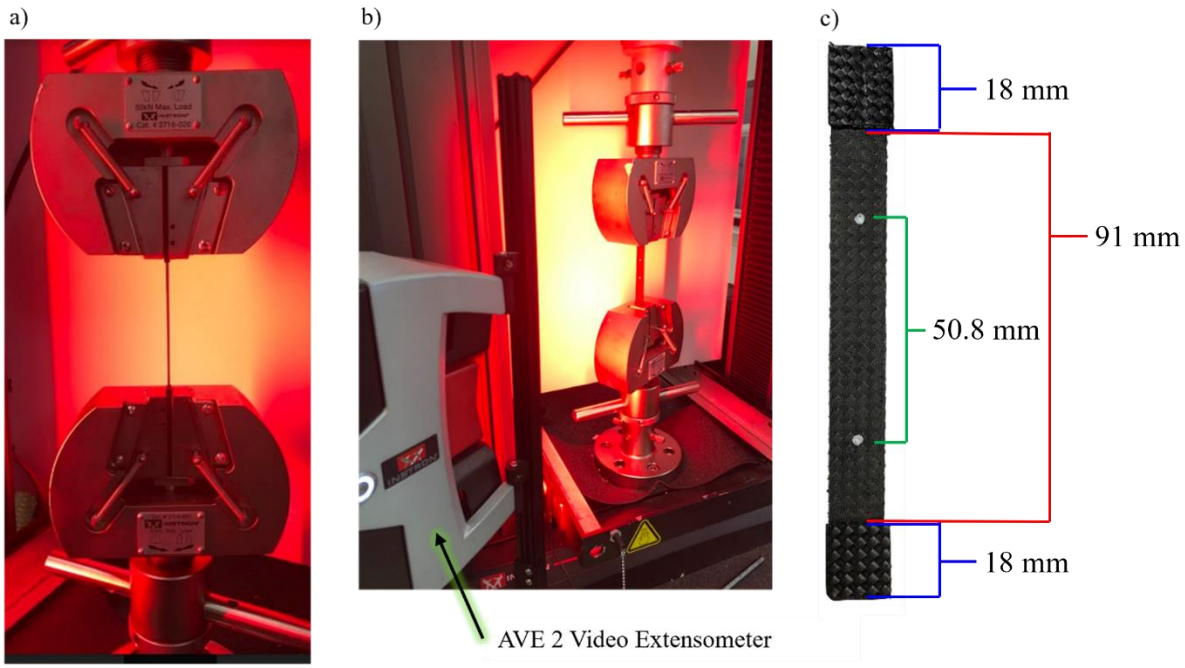

Figure 8: Tensile testing setup (a) Instron 5967 Universal Testing Frame tensile grips with specimen loaded; (b) Instron AVE 2 Non-Contacting Video Extensometer with tensile test setup; (c) CFRP tabbed tensile specimen.

3.6 Static Tensile Testing of Epoxy Specimens

Tensile specimens were type V according to ASTM D638. After hardener was added to the epoxy in a beaker, it was covered with a glass plate and placed in an ultrasonic water bath (Branson 1800) and degassed for five minutes before pouring into a silicone mold. Oven-cured specimens were immediately placed on a flat rack in a convection lab oven (Quincy Lab, Inc.) pre-heated to 110 °C and left for 12 hours. After 12 hours, the mold was removed from the oven and laid on a flat surface for 36 hours before removal of specimens and testing.

Static tensile testing was done in compliance with ASTM D638. All tension testing was performed on an Instron 5967 Universal Testing Frame with an Instron AVE 2 Non-Contacting

Video Extensometer. A gauge length encompassing the reduced parallel section of the specimen was marked for all specimens with a white paint marker to create a high-contrast image for the video extensometer. Testing of three specimens per type was done at a displacement rate of 1 mm per minute until failure. Equation 3.1 was used to calculate tensile strength.

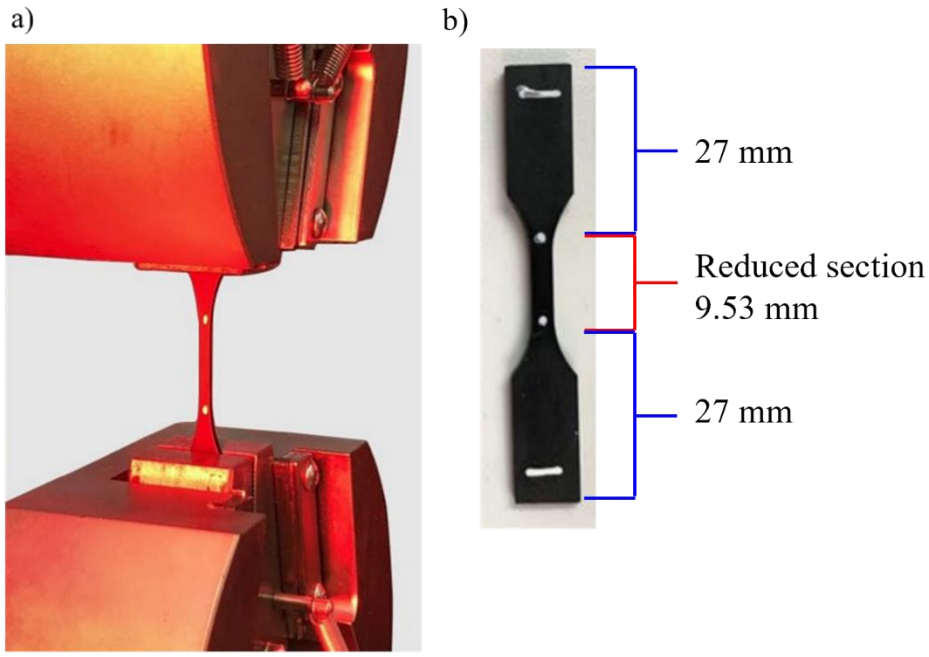

Figure 9: Epoxy tensile testing setup (a) Epoxy specimen loaded into tensile grips; (b) Epoxy specimen for tensile testing.

3.7 Peel Testing of CFRP

Peel testing of CFRP composites was done in accordance with ASTM D1876. Specimens were 25.4 mm wide, 12-layer CFRP designed to peel apart in between the sixth and seventh lamination. The procedure for manufacturing the CFRP composite for peel testing is outlined in Figure 10. The two halves of the composite formwork were L-shaped platforms made from wood, with a surface area larger than the specimen. The materials used in casting the composite were the same as those listed in the VAHT procedure. First, a layer of release film was taped to the surface

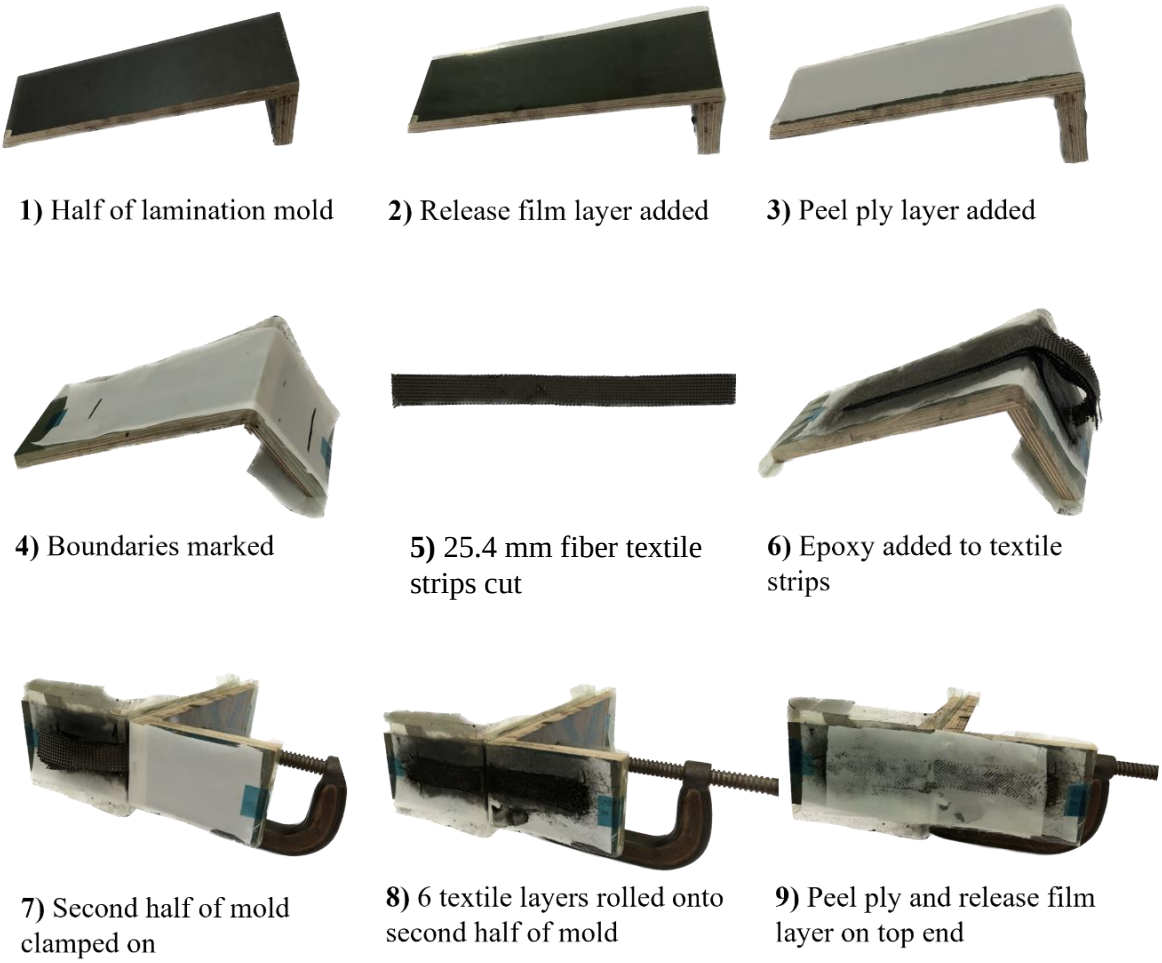

Figure 10: Steps for manufacturing CFRP composite for peel testing.

of the mold for easy release after hardening. Next, a layer of peel ply was taped on top of the release film. To create specimens to be about 230 mm along one length and about 76 mm along the shorter length as specified in ASTM D1876, a line was marked on the peel ply surface to indicate where to place the textile during lay-up. The same biaxial carbon fiber textile as specified in the VAHT procedure was used. 25.4 mm by 330 mm strips of carbon fiber textile were cut with a rotary blade. Prepared epoxy specified in the dispersion procedure was added to the epoxy hardener in a 2:1 ratio in a glass beaker. It was covered with a glass plate and placed in an ultrasonic water bath (Branson 1800) and degassed for five minutes. Carbon fiber strips were aligned with the marks on the composite mold and epoxy was pressed into the strips with a foam roller after each layer was placed until the layers were saturated. The first 6 layers of carbon fiber strips were pressed along the entire length down onto the mold. Layers 7 through 12 were only pressed down along the 230 mm length. The other half of the mold was then clamped on top of the composite along the 230 mm length with a metal C-clamp by hand until tight. The textile layers 7 through 12 that were not pressed down previously were folded over onto the other half of the mold and epoxy was pressed into those layers. A layer of peel ply and then a layer of release film was taped onto the short, top end of the mold. The mold was left for 48 hours at

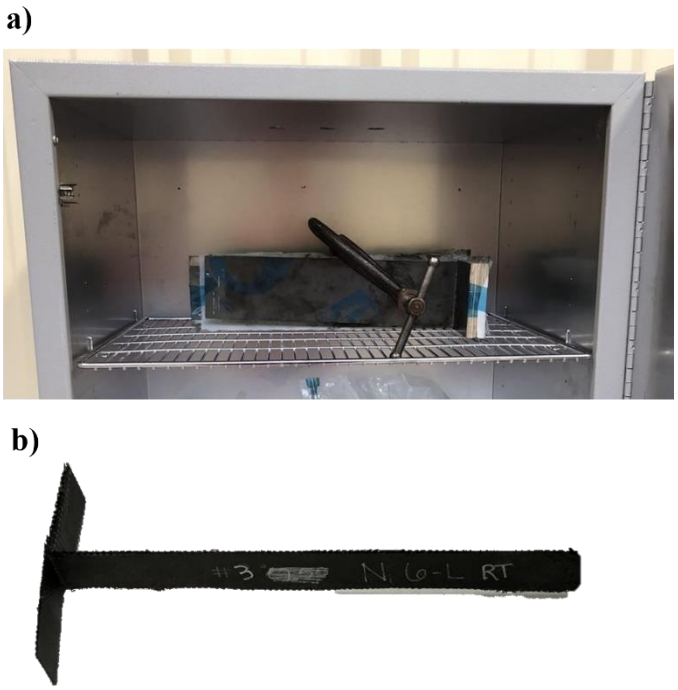

Figure 11: (a) Peel specimen in oven for curing; (b) Prepared peel specimen.

room temperature (30 ℃) before demolding. For specimens cured at elevated temperature, the mold was immediately placed onto a flat rack in a convection lab oven (Quincy Lab, Inc.) pre-heated to 110 ℃ and left for 24 hours. After 24 hours, the mold was removed from the oven and laid on a flat surface for 24 hours before removal of specimens and testing. Once de-molded, the shorter lengths of the specimen were trimmed down to 76.2 mm for a flat edge to better fit into the tensile grips.

Peel testing according to ASTM D1876 was performed on an Instron 5967 Universal Testing Frame. Testing of five specimens per type was done at a displacement rate of 20 mm per minute until the specimen peeled 127 mm along the length. The 127 mm mark along the length was marked with a white line prior to testing. The average peeling load for the first 127 mm after the initial load peak was calculated and used to find the interfacial adhesion.

$$Interfacial\ Adhesion\ Strength = \frac{Peeling\ Load}{w * t} \tag{3.2}$$

Where:

w = width of peel specimen

t = thickness of peel specimen

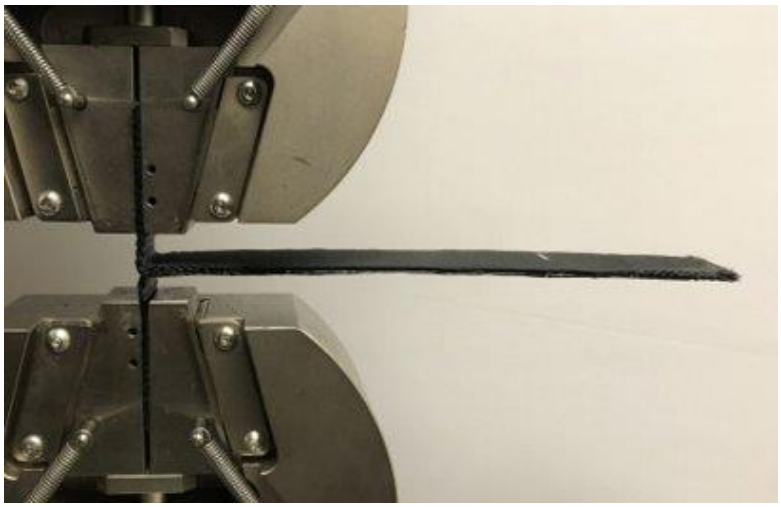

Figure 12: Peel specimen set up for testing.

3.8 Scanning Electron Microscopy (SEM) Imaging

Scanning Electron Microscope (SEM) imaging is a common method to look at the quality of CNT dispersal in the cured matrix. Individual nanotubes are too small to be seen with optical lens microscopes (Chakraborty et al. 2011). SEM uses an electron gun pointed towards a conductive specimen to create images based on reflected electron signals (Postek et al. 2013). Since epoxy is not conductive enough for this purpose, a thin coat of conductive metal is layered (called sputtering) onto the surface of the sample by electric charge.

A Zeiss Neon FE-SEM was used to capture images of room-temperature cured epoxy samples to evaluate the microstructure and distribution of CNTs. Specimens of isolated epoxy were fractured with a chisel to create a fracture plane where CNTs would be visible. An iridium sputter-coat was applied to all samples to enhance conductivity for image quality.

3.9 Differential Scanning Calorimetry (DSC)

Differential Scanning Calorimetry (DSC) is useful in identifying phase transition temperature of a polymer, including the glass transition temperature (Kodur et al. 2022). Based on how much thermal energy a sample absorbs compared to an inert sample baseline, specific heat of the sample can also be determined (Kodur et al. 2022). Additionally, DSC can be used to map the heat energy required for a polymer to cure. In this study, total heat of the reaction (enthalpy) was used as an indicator of curing level.

Empty aluminum pans and their respective lids were first weighed on a scale. 5-10 mg pieces of cured epoxy were chipped off the gauge length section of tensile specimens of each type and placed in the pan. For CFRP specimens, a small sliver of CFRP was cut off of the gauge length of tensile specimens. The pan was crimped closed using a crimper press (Perkin-Elmer) and the closed pan containing the sample was weighed to obtain sample weight. A TA Instruments Differential Scanning Calorimeter (DSC) 2500 shown in Figure 13 was used in conjunction with TRIOS software to perform DSC testing under dynamic conditions in a nitrogen atmosphere. The same calorimeter, software, and atmosphere conditions were used for all DSC tests. An empty pan served as a reference for measurements. After being placed in a DSC pan slot, The sample and reference pan were equilibrated to 40 °C and then heated to 300 °C with a ramp rate of 10 °C per minute. This temperature was held for 18 hours.



Figure 13: Differential Scanning Calorimeter

3.10 Thermogravimetric Analysis (TGA)

Thermogravimetric Analysis (TGA) measures the change in weight of a sample with change in temperature (Ng et al. 2018). A large drop in the weight of the sample can indicate degradation because volatile compounds form and evaporate during the decomposition of the sample (Ng et al. 2018). Mapping the degradation stages of a material can be useful for understanding the effects of environmental temperature changes.

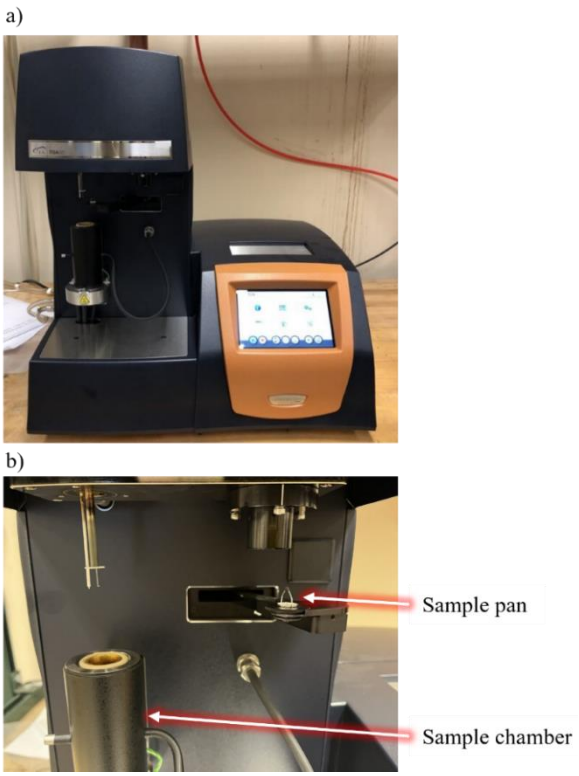

Figure 14: TGA Equipment: (a) TGA machine; (b) Sample pan and chamber.

TA Instruments Thermogravimetric Analysis (TGA) 55 machine shown in Figure 14 was used to perform testing. 5-10 mg pieces of cured epoxy were chipped off the gauge length section of tensile specimens of each type and placed onto the TGA machine pan. Sample weight was calculated by the TGA machine. The sample and reference pan were equilibrated to 25 °C. With a ramp rate of 10 °C per minute, the sample was heated to 800 °C under dynamic conditions. The TGA machine pan was heated with a torch and cooled in between samples to burn off any excess material to eliminate cross contamination.

Chapter 4: Experimental Results and Discussion

4.1 Effect of Nanomodification on CFRP Composites and Epoxy Matrices

Initial tensile testing of room-temperature cured CFRP results are shown in Figure 15, which displays the average tensile strength for each type of room temperature cured CFRP with varied MWCNT concentrations. Testing revealed that all nanomodified CFRP composite types chosen had, on average, lower tensile strength than neat CFRP composites. The functionalized-COOH 1% composite had the highest tensile strength among nanomodified composites and was similar to neat polymer tensile strength. The confidence level for this testing was 79%. Therefore, all additional testing was performed on neat, functionalized-COOH 1% (F 1%), and the respective

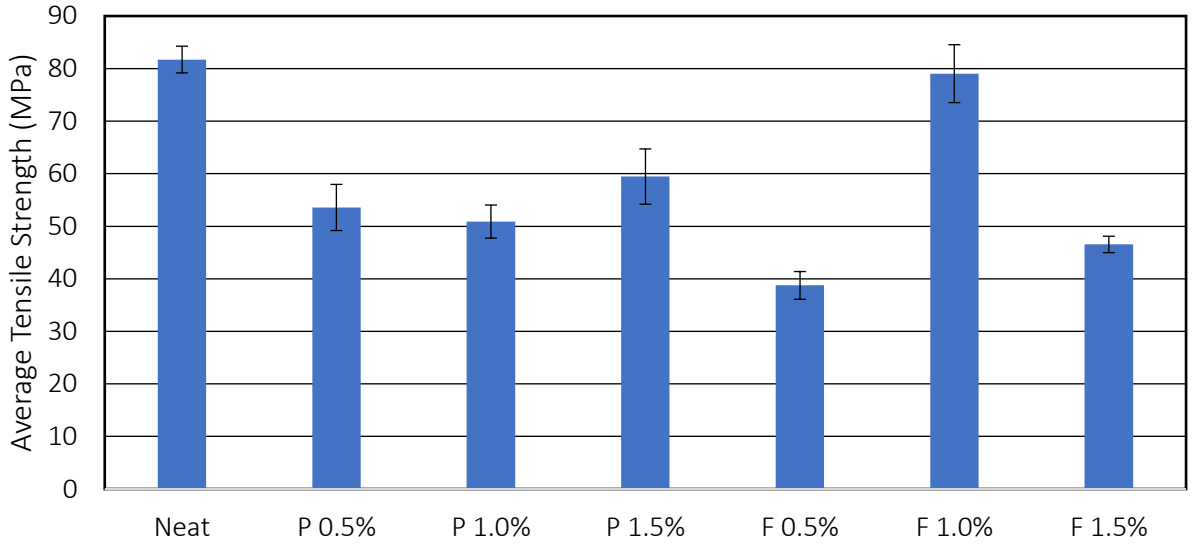

pristine CNT concentration (P 1%). Detailed results for this testing can be found in Table 2.

Figure 15: Average tensile strength of CFRP types (neat-N, pristine CNT-P, and functionalized-COOH – F).

Table 2: Results from static tensile testing of CFRP variations cured at different temperatures.

CFRP Type		**Strength (MPa)**	**Strain (%)**	**Young's Modulus (GPa)**
Neat RT	Mean	81.72	9.44	8.22
	Standard Deviation	4.27	1.15	0.85
	COV (%)	5.23	12.20	10.38
Pristine 0.5% RT	Mean (%)	53.57 (-34%)*	9.72 (3%)*	5.92 (-28%)*
	Standard Deviation	4.65	0.56	0.60
	COV (%)	8.70	5.77	10.14
Pristine 1% RT	Mean (%)	50.88 (-38%)*	7.58 (-20%)*	7.41 (10%)*
	Standard Deviation	3.45	1.13	0.78
	COV (%)	6.79	14.93	10.47
Pristine 1.5% RT	Mean (%)	59.45 (-27%)*	8.43 (-11%)*	6.44 (-22%)*
	Standard Deviation	3.67	0.94	0.38
	COV (%)	6.18	11.10	5.83
Functionalized-COOH 0.5% RT	Mean (%)	38.75 (-53%)*	7.36 (-22%)*	5.72 (-30%)*
	Standard Deviation	1.67	0.24	0.44
	COV (%)	4.31	3.23	7.69
Functionalized-COOH 1% RT	Mean (%)	79.03 (-3%)*	11.99 (27%)*	8.79 (7%)*
	Standard Deviation	2.51	1.39	1.27
	COV (%)	3.18	11.58	14.46
Functionalized-COOH 1.5% RT	Mean (%)	46.54 (-43%)*	7.40 (-22%)*	5.98 (-28%)*
	Standard Deviation	4.00	0.82	1.34
	COV (%)	3.18	11.58	14.46
Neat Oven	Mean (%)	75.87 (-7%)*	16.08 (70%)*	7.04 (-14%)*
	Standard Deviation	2.06	1.15	1.08
	COV (%)	2.72	7.14	15.31
Pristine 1% Oven	Mean (%)	74.66 (-9%)*	22.03 (133%)*	4.69 (-43%)*
	Standard Deviation	1.18	2.93	0.86
	COV (%)	1.58	13.27	18.43
Functionalized-COOH 1% Oven	Mean (%)	95.71 (17%)*	17.02 (80%)*	8.32 (1%)*
	Standard Deviation	2.05	0.27	2.65
	COV (%)	2.15	1.56	31.92

* Compared to neat RT.

To isolate the effects of nanomodification on the epoxy matrix of the FRP composite, static tension testing was performed on epoxy specimens with results in Figure 16 and a confidence level of 99%. For epoxy cured at room temperature (30 ℃), nanomodification with pristine 1% CNTs (P 1%) and functionalized-COOH 1% CNTs (F 1%) resulted in a lower average tensile strength and Young's modulus compared to neat epoxy. It was suspected that the cause of this lower strength was due to the changes in curing kinetics that resulted from the addition of CNTs to the epoxy. Strain at failure increased for nanomodified types compared to neat epoxy, aligning with literature that found CNTs to reduce vitrification in nanomodified epoxies (Dodiuk et al. 2022). The stress-strain curve in Figure 16(d) reveals a ductile behavior with yielding after the ultimate

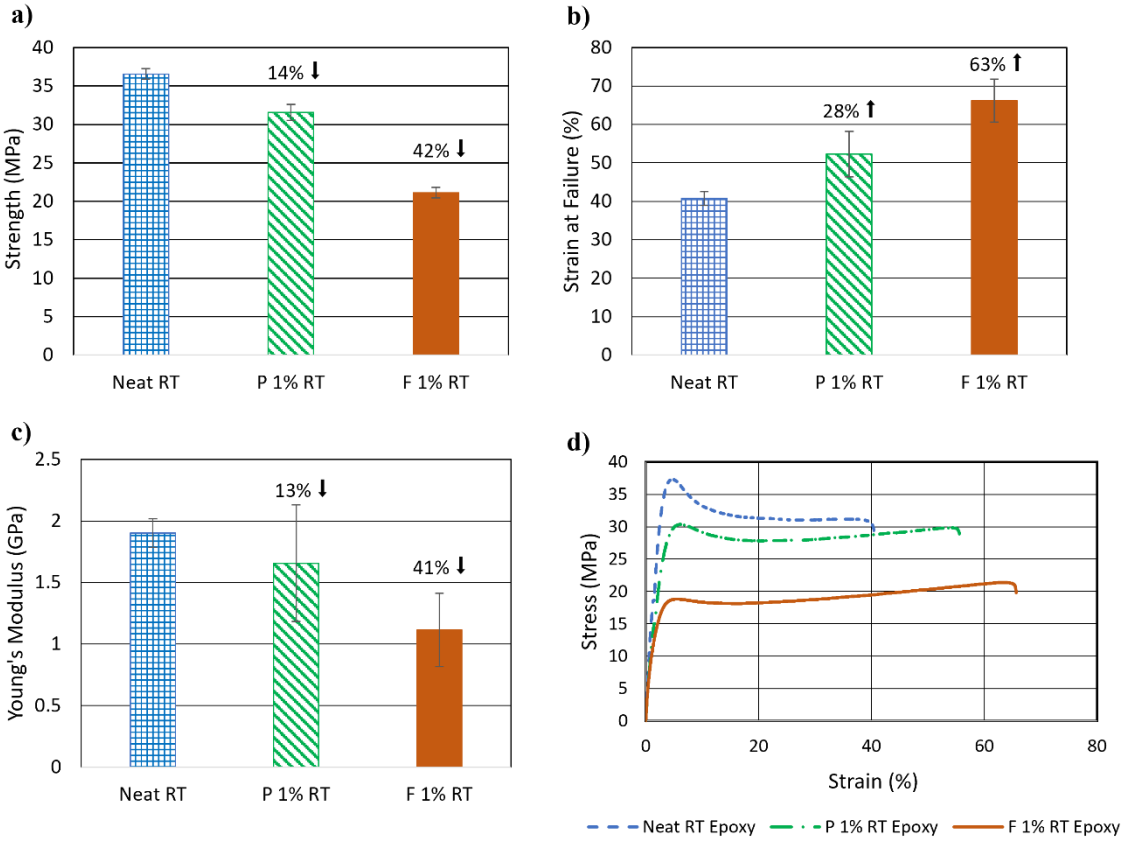

Figure 16: Mean (a) Tensile strength, (b) Strain at failure, (c) Young's Modulus, (d) Median stress-strain relationship of neat, pristine 1%, and functionalized 1% epoxy cured at room temperature.

strength for all epoxy types. Neat epoxy displayed a stronger, more brittle behavior than nanomodified counterparts, but is still relatively ductile.

Table 3: Results from tension tests done on epoxy cured at room temperature.

Epoxy Type		**Strength (MPa)**	**Strain (%)**	**Young's Modulus (GPa)**
Neat RT	Mean	36.55	40.75	1.90
	Standard Deviation	0.69	1.78	0.12
	COV (%)	1.88	4.37	6.14
Pristine 1% RT	Mean (%)	31.56 (-14%)*	52.33 (28%)*	1.66 (-13%)*
	Standard Deviation	1.02	5.92	0.47
	COV (%)	3.24	11.31	28.66
Functionalized-COOH 1% RT	Mean (%)	21.11 (-42%)*	66.22 (63%)*	1.12 (-41%)*
	Standard Deviation	0.69	5.56	0.30
	COV (%)	3.27	8.40	26.76

* Compared to Neat RT.

Both neat and nanomodified epoxy types failed along a plane perpendicular to the direction of loading shown in Figure 17. During testing, necking was observed before abrupt failure. Results from tension testing of room temperature cured nanomodified epoxy types shown in Table 2 indicate that nanomodification with either pristine or functionalized-COOH nanotubes decreases the strength and Young's modulus of the epoxy by a significant amount. However, the strain at failure decreases. Therefore, with nanomodification, the epoxy became less stiff and is more easily deformed at lower loading. The epoxy was most affected by functionalized-COOH CNTs, with an average decrease in strength of 42% and an increase in strain of 63%.



Figure 17: Representative neat (top) and nanomodified (bottom) epoxy resin specimens after tensile testing.

Results from static tensile testing of CFRP composites cured at room temperature shown in Figure 18 with a confidence level of 79% indicate that the CFRP composites did not mirror the mechanical behavior of the isolated epoxy matrices. This could be due to the interaction between the carbon fiber and matrix components. The carbon fiber textile physically impedes the curing reaction of the epoxy when it takes up space in the matrix, leading to potentially lower quality of polymerization and curing. Additionally, the sizing, a chemical coating meant to keep fibers together during handling, applied to the carbon fiber during manufacturing can affect the bonding potential between fibers and the epoxy matrix by changing the chemical groups left on the surface and therefore the reactivity with other molecules (Eyckens et al. 2020). The details of sizing are typically proprietary and the details on sizing of the carbon fiber used is unavailable. For CFRP, only the P 1% CNT composite decreased significantly in strength, strain at failure and Young's modulus, while the F 1% CNT composite decreased in strength only slightly and increased in strain at failure and Young's modulus compared to neat CFRP. The significant drop in mechanical properties of the P 1% CNT composite is suggestive of an incompatibility between the carbon fiber, or its sizing, and pristine CNT modified epoxy matrix, while the increase in strain for the F 1% composite points to strong interfacial bonding between the CNTs, epoxy matrix, and carbon fiber. While neat and F 1% CNT epoxy displayed noticeably different behaviors, F 1% CNT CFRP exhibited performance similar to neat CFRP. The neat CFRP composite maintained the highest strength but could not deform as much as the nanomodified composites before failure.

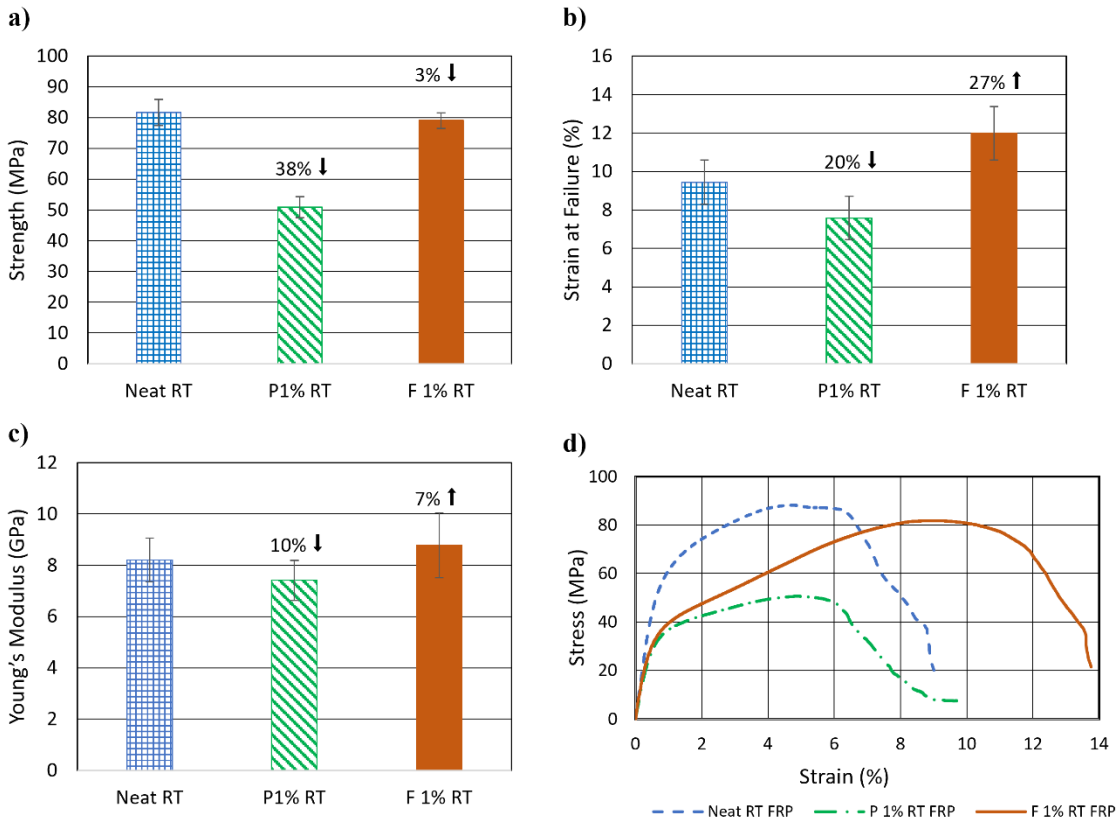

Figure 18: Mean (a) tensile strength, (b) strain at failure, (c) Young's modulus, and (d) median stress-strain relationship of neat, pristine 1%, and functionalized 1% CFRP cured at room temperature.

Table 4: Results from tension tests done on CFRP cured at room temperature.

CFRP Type		**Strength (MPa)**	**Strain (%)**	**Young's Modulus (GPa)**
Neat RT	Mean Value	81.72	9.44	8.22
	Standard Deviation	4.27	1.15	0.85
	COV (%)	5.23	12.20	10.38
Pristine 1% RT	Mean Value (%)	50.88 (-38%)*	7.58 (-20%)*	7.41 (-10%)*
	Standard Deviation	3.45	1.13	0.78
	COV (%)	6.79	14.93	10.47
Functionalized-COOH 1% RT	Mean Value (%)	79.03 (-3%)*	11.99 (27%)*	8.79 (7%)*
	Standard Deviation	2.51	1.39	1.27
	COV (%)	3.18	11.58	14.46

* Compared to Neat RT.

Failure of the CFRP composites was consistent with fiber-matrix debonding as predicted. During tensile testing, the parallel section of the specimen reduced in width with elongation. Fibers slowly debonded from the matrix during loading until complete failure shown in Figure 19. Minimal fiber damage is visible in the specimens along the failure plane, indicating the failure was mostly controlled by the matrix-fiber debonding instead of fiber breakage. Overall, the properties of epoxy did not translate to CFRP. In testing to understand the composite behavior, testing of the isolated epoxy matrix alone is not adequate to predict the effect of nanomodification in FRP composites.



Figure 19: (a) Representative CFRP tensile specimen after failure; (b) Failure mode of CFRP tensile specimen.

To further understand the mechanical behavior of nanomodified CFRP composites, peel testing was conducted with a resulting confidence level of 98%. As shown in Figure 20, nanomodification of the CFRP peel specimens increased the mean interfacial adhesion strength significantly. CNTs are suspected to bridge interlaminar gaps in the composite, increasing the load capacity of the composite as long as the layers remain together. P 1% and F 1% composites performed similarly for peel testing, and all specimens failed in the epoxy layer of the peel interface. There was no indication of fiber damage or breakage on the surface of the peel interface shown in Figure 20 (b). However, the interface was rough due to the epoxy peaks and flakes created from damage during testing.

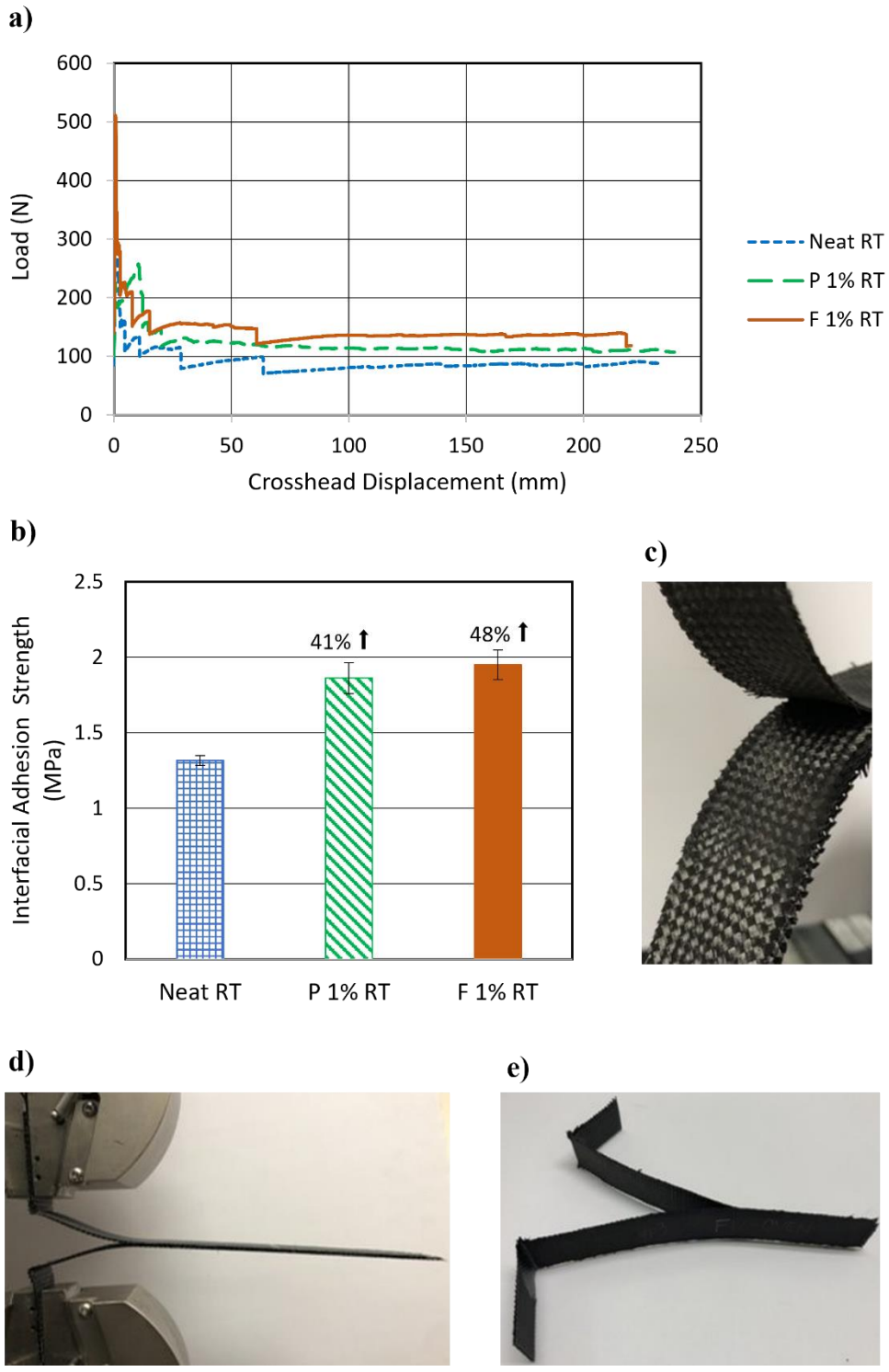

Figure 20: (a) Stress-strain relationship, (b) mean interfacial adhesion strength, (c) peel interface, (d) specimen during testing, and (e) specimen after failure for neat, pristine 1%, and functionalized 1% CFRP cured at room temperature.

Table 5: Results from peel tests done on CFRP cured at room temperature.

CFRP Type		**Interfacial Adhesion Strength (MPa)**
Neat RT	Mean	1.32
	Standard Deviation	0.03
	COV (%)	2.52
Pristine 1% RT	Mean (%)	1.86 (41%)*
	Standard Deviation	0.10
	COV (%)	5.51
Functionalized-COOH 1% RT	Mean (%)	1.95 (48%)*
	Standard Deviation	0.10
	COV (%)	5.00

* Compared to Neat RT.

4.2 Effect of Curing Temperature of CFRP Composites and Epoxy Matrices

As nanomodified CFRP composites were expected to have higher tensile strength than neat composites, the curing kinetics of nanomodified epoxies was investigated further. It was suspected that the CNTs absorb energy in the curing reaction and therefore nanomodified epoxies need additional energy during the reaction for the mixture to cure to a higher degree. Static tensile testing was performed on epoxy and CFRP composites cured this time at 110 °C. Stress-strain responses from static tensile testing of neat, P 1%, and F 1% epoxy are shown in Figure 21 and results are shown in Table 6. When cured at elevated temperature, the epoxy became stiffer with a higher Young's modulus and did not display the ductile behavior of room temperature-cured specimens. Instead, the epoxy was brittle during failure, but displayed much higher strength. The visible failure modes of specimens did not change when cured at elevated temperature. Figure 17 is representative of the epoxy failure at both curing temperatures.

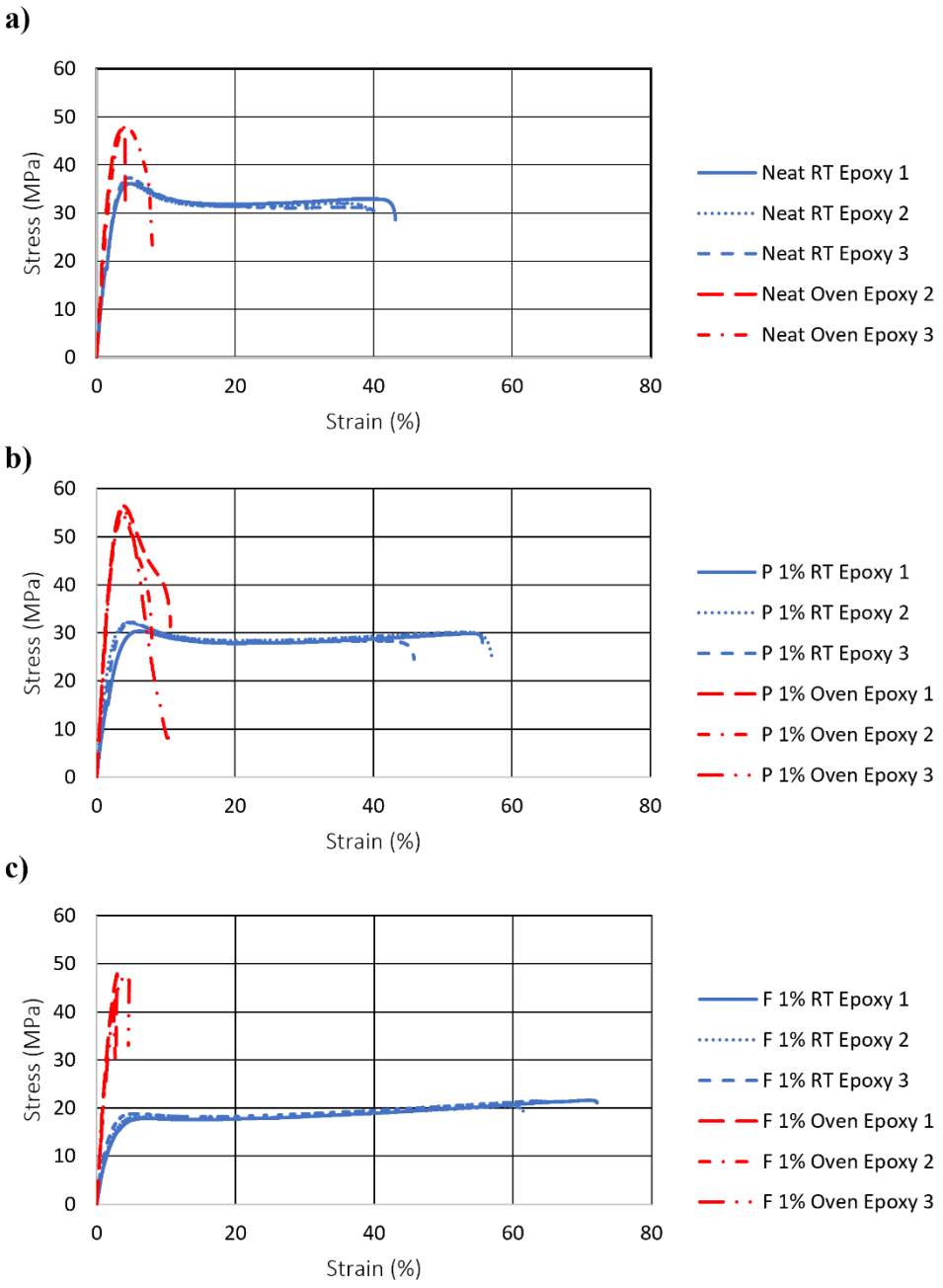

Figure 21: Stress-strain relationship for (a) neat epoxy, (b) pristine CNT epoxy (1% wt. of epoxy), and (c) functionalized-COOH CNT epoxy (1% wt. of epoxy) cured at room temperature (30 °C) and elevated oven temperature (110 °C).

Table 6: Results from static tension tests on nanomodified epoxy cured at room temperature (RT, 30℃) and oven temperature (Oven, 110 ℃).

Epoxy Type		**Strength (MPa)**	**Strain (%)**	**Young's Modulus (GPa)**
Neat RT	Mean	36.55	40.75	1.90
	Standard Deviation	0.69	1.78	0.12
	COV (%)	1.88	4.37	6.14
Pristine 1% RT	Mean (%)	31.56 (-14%)*	52.33 (28%)*	1.66 (-13%)*
	Standard Deviation	1.02	5.92	0.47
	COV (%)	3.24	11.31	28.66
Functionalized-COOH 1% RT	Mean (%)	21.11 (-42%)*	66.22 (63%)*	1.12 (-41%)*
	Standard Deviation	0.69	5.56	0.30
	COV (%)	3.27	8.40	26.76
Neat Oven	Mean (%)	47.94 (31%)*	5.82 (-86%)*	2.10 (11%)*
	Standard Deviation	1.40	5.59	0.91
	COV (%)	2.94	96	0.43
Pristine 1% Oven	Mean (%)	55.38 (52%)*	9.59 (-76%)*	2.70 (42%)*
	Standard Deviation	1.09	1.49	0.12
	COV (%)	1.96	15.54	4.51
Functionalized-COOH 1% Oven	Mean (%)	45.76 (25%)*	3.33 (-92%)*	2.29 (21%)*
	Standard Deviation	3.04	1.22	0.10
	COV (%)	6.65	36.76	4.43

* Compared to Neat RT.

Table 7: Percent increase of mechanical properties of epoxy with respect to respective CNT types when cured at 110 ℃ instead of 30 ℃.

	Tensile Strength	**Strain at Failure**	**Young's Modulus**
Neat	31%	-86%	11%
Pristine 1%	75%	-80%	63%
Functionalized-COOH 1%	117%	-101%	104%

Shown in Figure 22, all types of epoxies increased in tensile strength with the increase in curing temperature. However, the increase in tensile strength of nanomodified epoxies is significantly more, with F 1% epoxy increasing the most in tensile strength, by 117%, when cured at elevated temperature. Similarly, all types increased in Young's modulus, with neat increasing

the least and F 1% increasing the most by 104%. Curing at elevated temperature decreased the strain at failure for all epoxy types significantly. Again, F 1% changed the most with a 101% decrease. All variants of epoxy cured at elevated temperature were stronger than neat epoxy cured at room temperature, but neat epoxy strength only increased by 11%. The significant difference in the effect of curing temperature on neat versus nanomodified variants supports the hypothesis that additional energy for nanomodified composites, in this case in the form of heat, is critical during the curing reaction in order to reach full potential and interfacial engagement. Higher coefficients of variation are explained by CNT agglomerates that interrupt the homogeneous matrix. Agglomerates that interrupt the matrix act as a weak spot and cracks tend to propagate around them.

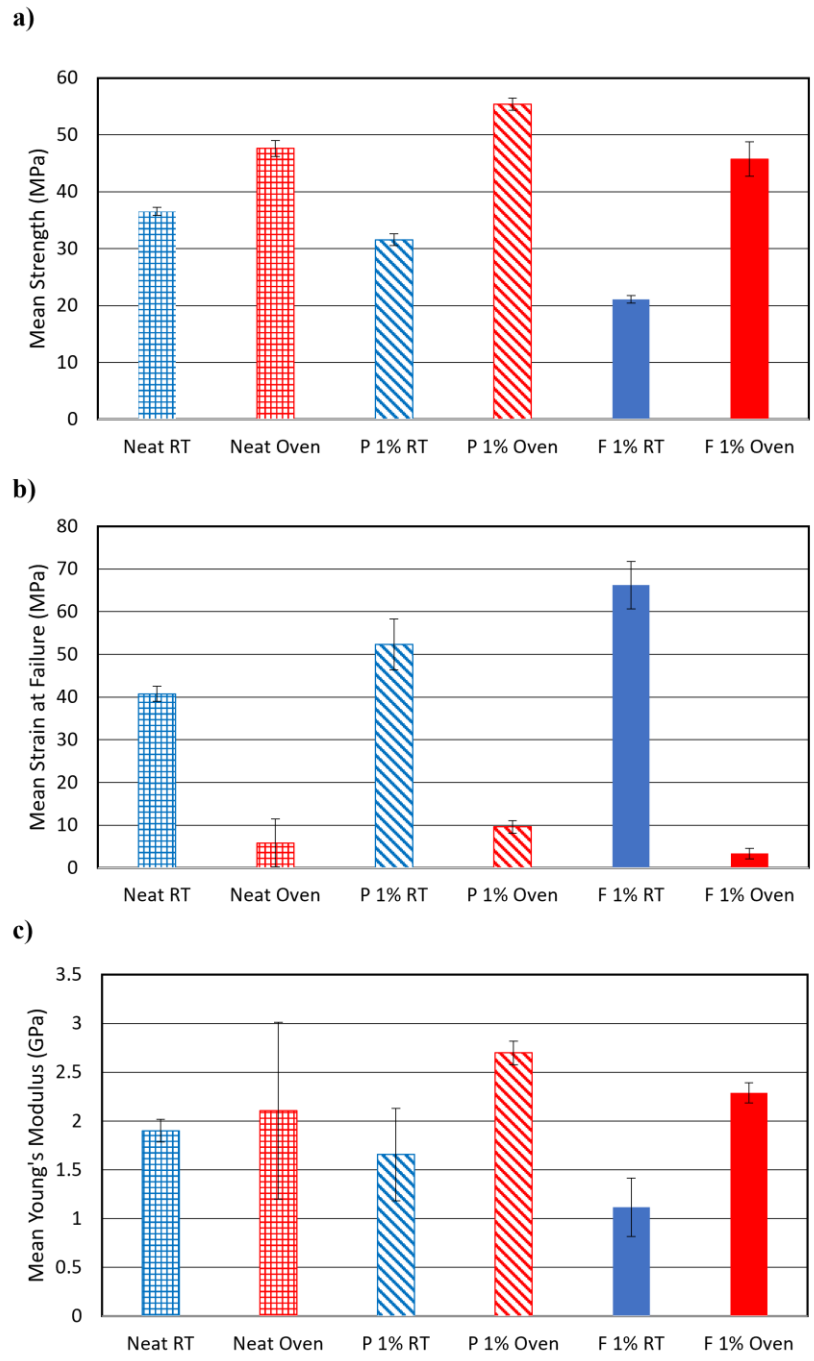

Figure 22: Mean (a) tensile strength, (b) strain at failure, and (c)Young's Modulus of epoxy resin cured at room temperature (30 ℃) and elevated temperature (110 ℃).

Tensile testing on CFRP composites cured at 110 ℃ was also performed to evaluate the effect of curing temperature on composite behavior. Figure 23 shows the stress-strain relationship

between room temperature (30 ℃) cured and oven (110 ℃) cured CFRP composites for neat, P 1%, and F 1% variations. Failure type did not change significantly, with a period of yielding before failure. Figure 19 is representative of CFRP failure for both curing temperatures.

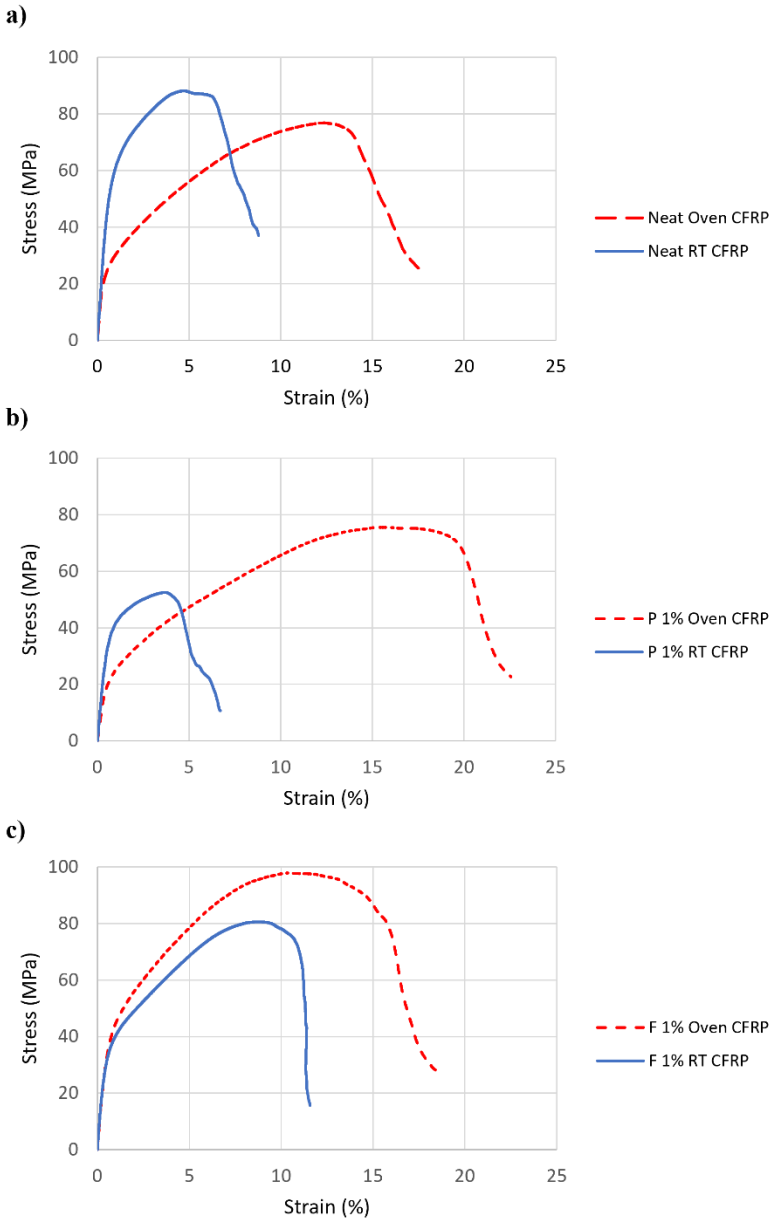

Figure 23: Stress-strain relationship for median (a) neat CFRP, (b) pristine CNT CFRP (1% wt. of epoxy), and (c) functionalized-COOH CNT CFRP (1% wt. of epoxy) cured at room temperature (30 ℃) and elevated oven temperature (110 ℃).

Table 8: Results from static tension tests on nanomodified CFRP cured at room temperature (RT, 30℃) and oven temperature (Oven, 110 ℃).

CFRP Type		Strength (MPa)	Strain (%)	Young's Modulus (GPa)
Neat RT	Mean	81.72	9.44	8.22
	Standard Deviation	4.27	1.15	0.85
	COV (%)	5.23	12.20	10.38
Pristine 1% RT	Mean (% increase)	50.88 (-38%)	7.58 (-20%)	7.41 (10%)
	Standard Deviation	3.45	1.13	0.78
	COV (%)	6.79	14.93	10.47
Functionalized-COOH 1% RT	Mean (% increase)	79.03 (-3%)	11.99 (27%)	8.79 (7%)
	Standard Deviation	2.51	1.39	1.27
	COV (%)	3.18	11.58	14.46
Neat Oven	Mean (% increase)	75.87 (-7%)	16.08 (70%)	7.04 (-14%)
	Standard Deviation	2.06	1.15	1.08
	COV (%)	2.72	7.14	15.31
Pristine 1% Oven	Mean (% increase)	74.66 (-9%)	22.03 (133%)	4.69 (-43%)
	Standard Deviation	1.18	2.93	0.86
	COV (%)	1.58	13.27	18.43
Functionalized-COOH 1% Oven	Mean (% increase)	95.71 (17%)	17.02 (80%)	8.32 (1%)
	Standard Deviation	2.05	0.27	2.65
	COV (%)	2.15	1.56	31.92

* Percent increase compared to Neat RT.

Table 9: Percent increase of mechanical properties of CFRP with respect to respective CNT types when cured at 110 ℃ instead of 30 ℃.

	Tensile Strength	Strain at Failure	Young's Modulus
Neat	-7%	70%	-14%
Pristine 1%	47%	190%	-37%
Functionalized-COOH 1%	21%	42%	-5%

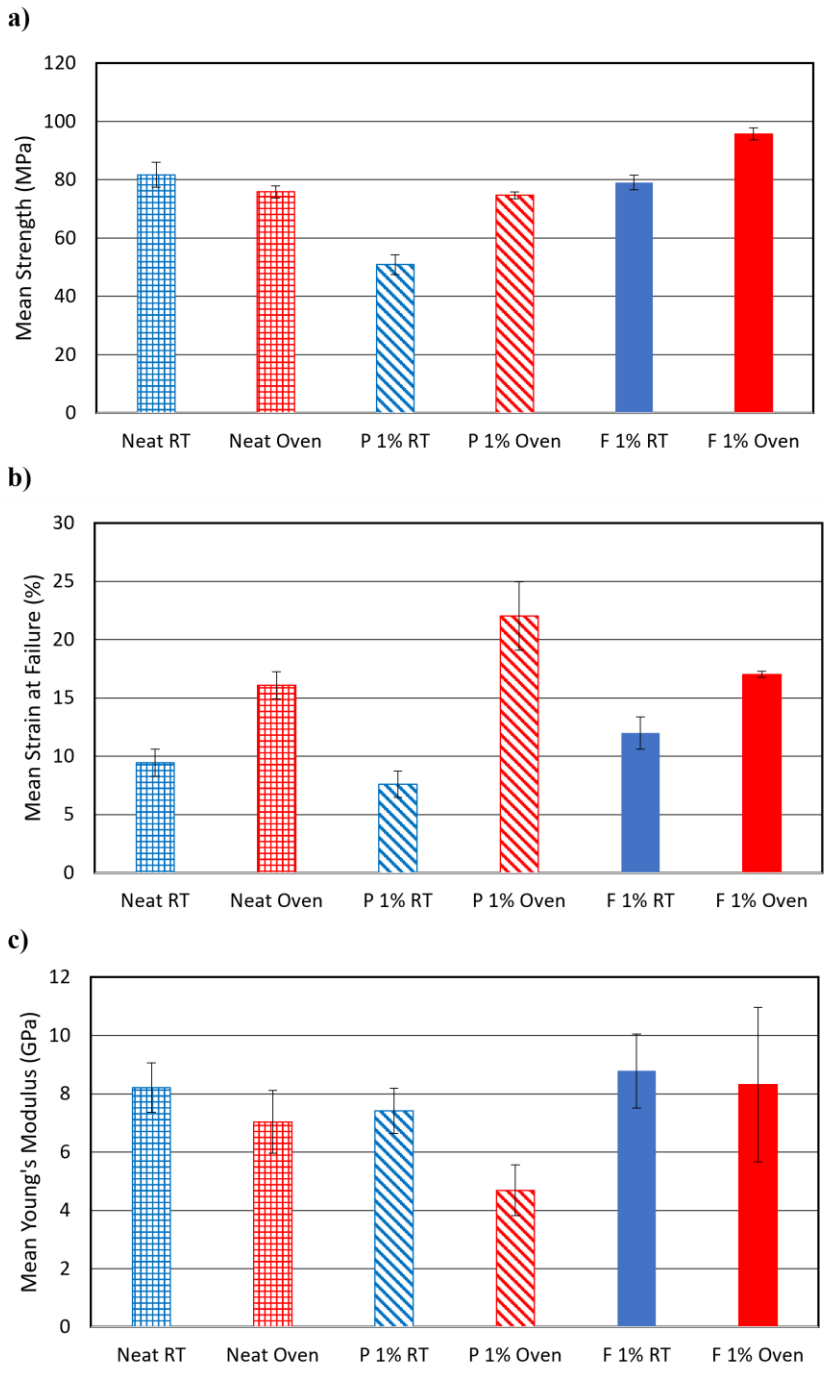

Figure 24: Mean (a) tensile strength, (b) strain at failure, and (c)Young's modulus of CFRP cured at room temperature (30 ℃) and elevated temperature (110 ℃).

Shown in Figure 24, Nanomodified CFRP composite strain at failure increased significantly, whereas the epoxy strain decreased with an increase in curing temperature. Similarly,

the Young's modulus of all the CFRP composites decreased while the epoxy modulus increased with an increase in curing temperature. If cured at elevated temperatures, F 1% CFRP composite has a higher tensile strength than neat CFRP cured at either room temperature or elevated temperature. However, P 1% composite still has a lower tensile strength than neat CFRP cured at either temperature. Overall, elevating curing temperature of nanomodified CFRP increases tensile strength and strain at failure, while decreasing the elastic modulus.

Interfacial adhesion for all CFRP variations was also tested for CFRP cured at 110 ℃. Results for peel testing are shown in Table 10 and Figure 25.

Table 10: Results from peel tests on nanomodified CFRP cured at room temperature (RT, 30℃) and oven temperature (Oven, 110 ℃).

CFRP Type		**Interfacial Adhesion Strength (MPa)**
Neat RT	Mean	1.32
	Standard Deviation	0.03
	COV (%)	2.52
Pristine 1% RT	Mean (%)	1.86 (41%)*
	Standard Deviation	0.10
	COV (%)	5.51
Functionalized-COOH 1% RT	Mean (%)	1.95 (48%)*
	Standard Deviation	0.10
	COV (%)	5.00
Neat Oven	Mean (%)	1.02 (-23%)*
	Standard Deviation	0.05
	COV	5.25
Pristine 1% Oven	Mean (%)	2.14 (62%)*
	Standard Deviation	0.32
	COV	15.09
Functionalized-COOH 1% Oven	Mean (%)	3.04 (130%)*
	Standard Deviation	0.34
	COV	11.32

* Compared to Neat RT.

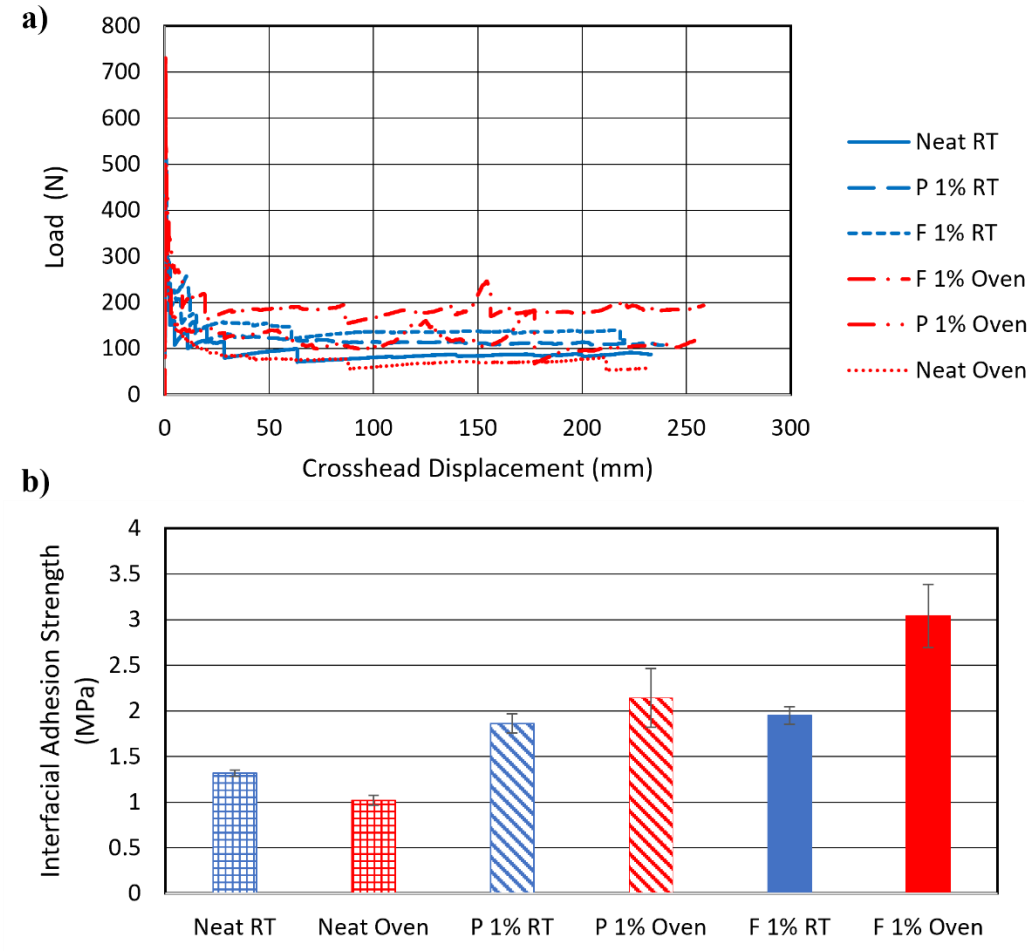

Figure 25: (a) Load-crosshead displacement relationship and (b) mean interfacial adhesion strength for CFRP cured at room temperature (30 ℃) and elevated temperature (110 ℃).

Interfacial adhesion strength increased for all nanomodified CFRP composites while decreasing for neat CFRP. This is likely because the elevated curing temperature is allowing the MWCNTs to correctly bond within the epoxy matrix, enabling them to bridge microcracks as intended. However, nanomodified CFRP types achieved a higher interfacial adhesion strength than neat CFRP regardless of curing temperature.

Table 11: Percent increase of interfacial adhesion strength of CFRP with respect to respective CNT types when cured at 110 ℃ instead of 30 ℃.

	Interfacial Adhesion Strength
Neat	-23%
Pristine 1%	15%
Functionalized-COOH 1%	56%

In many structural applications, interfacial adhesion is critical, and therefore it is likely not beneficial to cure neat CFRP at elevated temperatures if high interfacial strength is desired. F 1% CFRP variation had the highest interfacial adhesion strength and increased in tensile strength the most with oven-curing.

4.3 CNT Dispersion Quality and SEM

SEM imaging of room temperature cured epoxy was used to check CNT dispersion quality and identify any damage to the CNTs, and results are shown in Figure 26. Images of the neat epoxy are shown in Figure 26(a) and (b). Figure 26(c) shows one of the CNT agglomerations throughout epoxy samples and Figure 26(d) shows a higher magnification view of this agglomeration. However, all agglomerations were similar to sizes found acceptable in other existing literature (Robiul Islam et al. 2019). It is acceptable to see CNT agglomerates in a matrix as long as there are few and they are not large. Overall, dispersion of CNTs in both types of nanomodified epoxy appears acceptable.

Single MWCNTs can be seen protruding from the epoxy. The aspect ratio of the CNT appears undamaged, confirming that the ultrasonication procedure did not damage the CNTs during dispersion. In Figure 26(h), CNTs can be seen bridging a cavity in the epoxy. The ability of the CNTs to reach across small cracks or pores like this one is what allows the increase in tensile

and interfacial adhesion strength if properly engaged within the matrix. Additionally, Figure 26(f) and (g) show that some of the functionalized-COOH CNTs sticking out of the matrix appear broken off. This is an indication that matrix-CNT interfacial bonding was strong and did not allow the CNTs to pull out of the matrix during rupture. Conversely, in Figure 26 (e) showing pristine CNTs, there are less broken CNTs, a sign that the pristine CNTs may not have bonded as well in the epoxy matrix.

a)

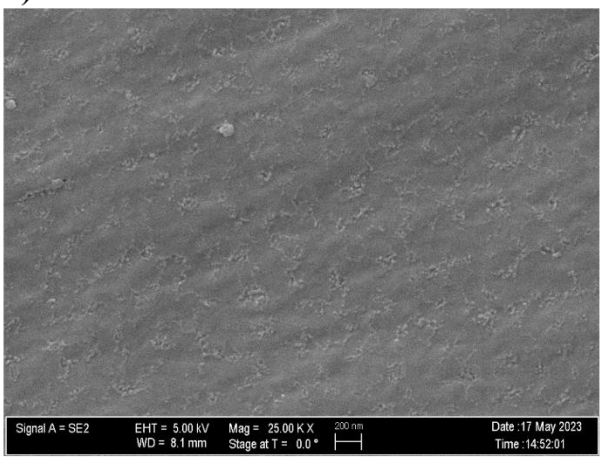
Signal A = SE2
EHT = 5.00 kV
WD = 8.1 mm
Mag = 25.00 K X
Stage at T = 0.0 °
200 nm
Date :17 May 2023
Time :14:52:01

b)

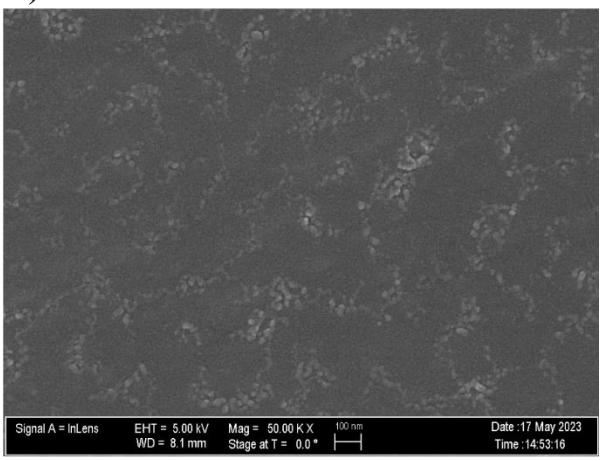
Signal A = InLens
EHT = 5.00 kV
WD = 8.1 mm
Mag = 50.00 K X
Stage at T = 0.0 °
100 nm
Date :17 May 2023
Time :14:53:16

c)

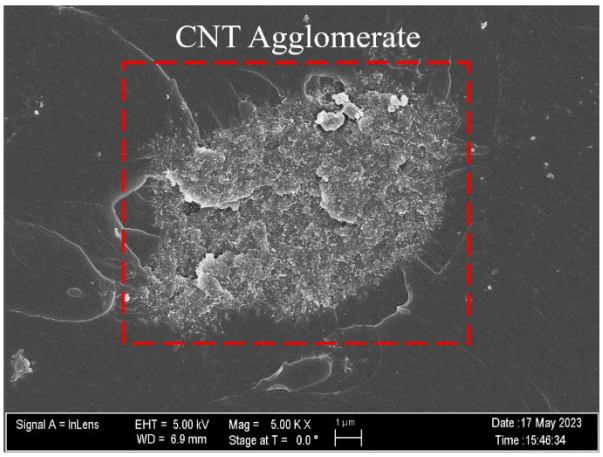
CNT Agglomerate
Signal A = InLens
EHT = 5.00 kV
WD = 6.9 mm
Mag = 5.00 K X
Stage at T = 0.0 °
1 µm
Date :17 May 2023
Time :15:46:34

d)

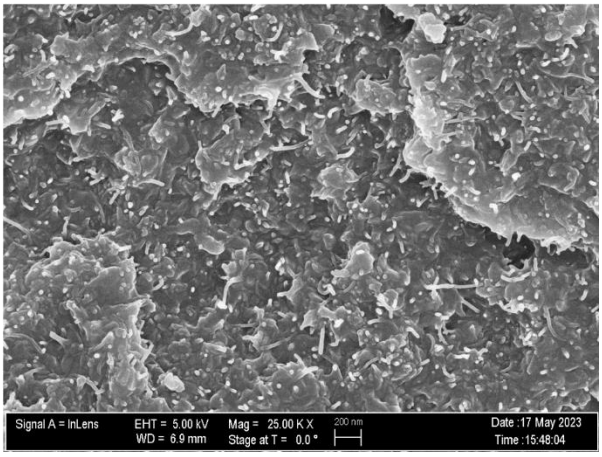
Signal A = InLens
EHT = 5.00 kV
WD = 6.9 mm
Mag = 25.00 K X
Stage at T = 0.0 °
200 nm
Date :17 May 2023
Time :15:48:04

e)

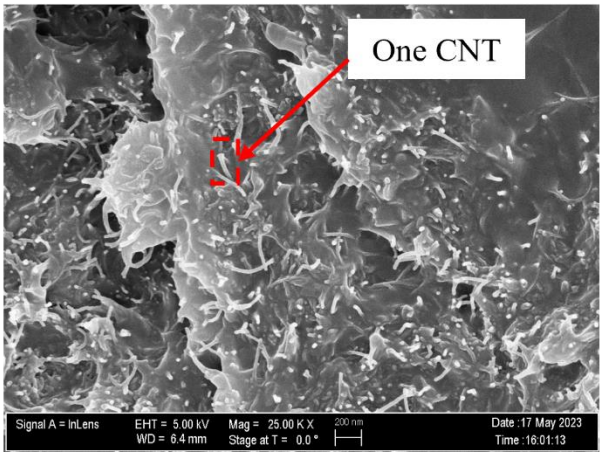
One CNT
Signal A = InLens
EHT = 5.00 kV
WD = 6.4 mm
Mag = 25.00 K X
Stage at T = 0.0 °
200 nm
Date :17 May 2023
Time :16:01:13

f)

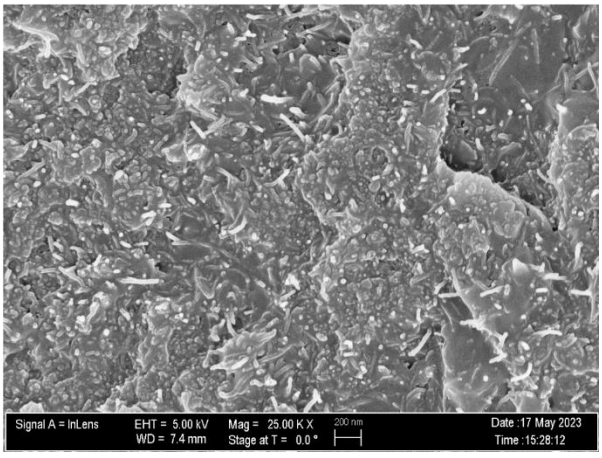
Signal A = InLens
EHT = 5.00 kV
WD = 7.4 mm
Mag = 25.00 K X
Stage at T = 0.0 °
200 nm
Date :17 May 2023
Time :15:28:12

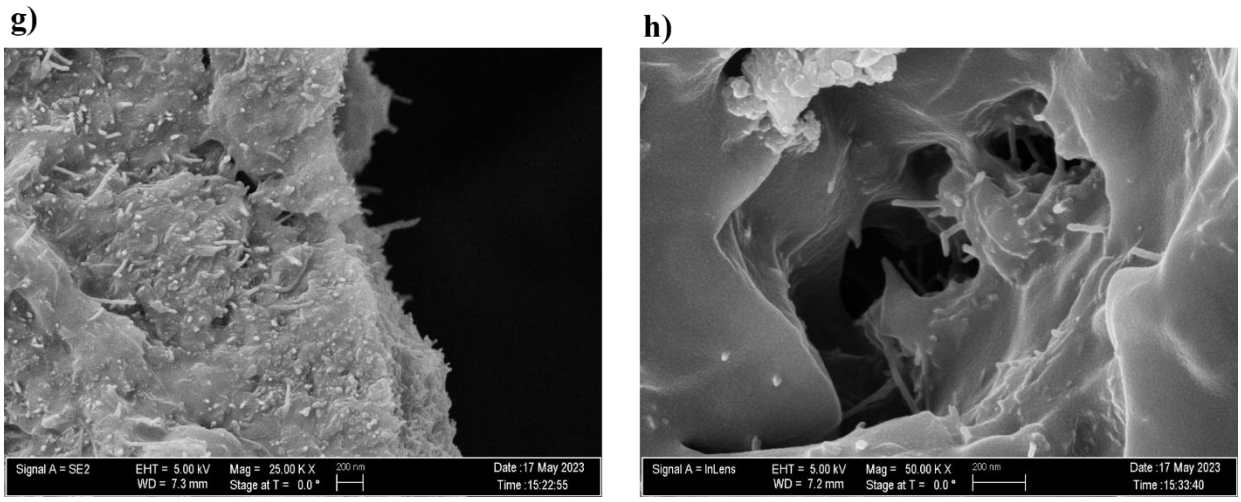

Figure 26: SEM images of (a) neat 25K X, (b) neat 50K X, (c) pristine CNT 5K X, (d) pristine CNT 25K X, (e) pristine CNT 25K X, (f) functionalized-COOH CNT 25K X, (g) functionalized-COOH CNT 25K X, (h) functionalized-COOH CNT 50K X epoxy cured at room temperature.

4.4 TGA

TGA was performed on cured epoxy samples of the six epoxy variations. Results are shown in Figure 27, which indicates that neat room temperature cured, neat oven cured, F 1% room

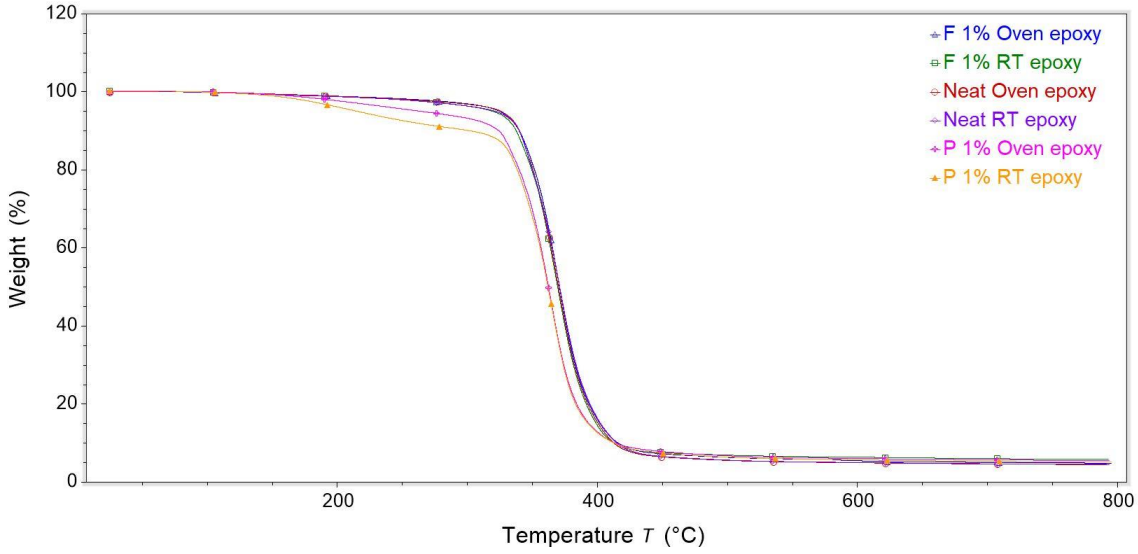

Figure 27: TGA results for all epoxy types.

temperature cured, and F 1% oven cured samples had similar thermal stability. However, P 1% samples initially lost weight at a much lower temperature than other types of epoxies, indicating lower thermal stability.

The residue left in the pan after TGA has run is mostly the CNTs that have higher thermal stability than the epoxy. When the epoxy is burned off, the CNTs remain. Therefore, a higher percentage of residue is left in the nanomodified samples. The interpolated temperatures of onset and end of weight loss shown in Table 12 were calculated by TRIOS software and are similar for all sample types, but slightly lower for the P 1% variation. Incorporation of pristine and functionalized-COOH MWCNTs into the epoxy matrix decreased the decomposition temperature compared to neat room temperature-cured epoxy, but pristine MWCNTs decreased the temperature most significantly. Curing neat epoxy at elevated temperature also decreased the decomposition temperature (Hesami et al. 2014).

Table 12: Onset and end of weight loss from TGA for all epoxy types.

	Onset of Weight Loss Temperature (°C)	End of Weight Loss Temperature (°C)
Neat RT	343	396
Neat Oven	343	394
P 1% RT	336	386
P 1% Oven	336	386
F 1% RT	343	393
F 1% Oven	345	395

4.5 DSC

Results from DSC testing shown in Figure 28 were used to calculate normalized heat/enthalpy by integrating the area under the heat flow curve normalized with sample mass over

the temperature range. Higher amounts of enthalpy, or heat energy, from a sample indicate a lower degree of curing (Kosukegawa 2018). Between room and elevated temperature curing, characteristic shifts in the DSC curves are present, evident by the changes in peak temperature in the peaks highlighted in Figure 28. When the polymer chains are more loosely linked, as is the case in an epoxy with a low degree of cure, the heat flow through the sample is higher. Conversely, the more rigid polymer structures characteristic of a well-cured epoxy allow less heat to flow through the sample (Eurofins Scientific 2023).

For all epoxy samples, those cured at elevated oven temperature had a lower normalized enthalpy. Therefore, curing epoxy at elevated temperature increased the degree of cure for all types. Additionally, difference in enthalpy between oven and room temperature cured epoxies was greater for nanomodified epoxies. Between room temperature cured epoxies, F 1% epoxy had higher degree of cure than neat epoxy, indicating that the addition of functionalized-COOH MWCNTs to the epoxy increases the degree of cure without changing environmental curing temperature. However, the addition of pristine MWCNTs decreased the degree of cure for room temperature cured epoxy. Another characteristic of the DSC curve is the peak temperature that indicates an exothermic reaction that happens during polymerization. The peak temperature did not change significantly for F 1% epoxy between room temperature and oven cured specimens, but between Neat and P 1% samples, the peak temperature shifted noticeably. For neat epoxy variations, room temperature cured epoxy had a lower peak temperature while for nanomodified epoxies, oven cured epoxy had a lower peak temperature. This indicates that crystallization in the polymer happened at a lower temperature for neat epoxy compared to nanomodified epoxies. Further, P 1% had the highest peak temperatures for both curing types. For CFRP samples, neat

and P 1% CFRP cured at elevated temperature had lower enthalpy and therefore higher degree of curing. However, F 1% CFRP cured better in room temperature conditions. The peak temperatures of nanomodified CFRP were lower for oven cured variations, while the peak temperature of neat CFRP was higher for room temperature cured variations. Therefore, the polymer crystallization happened at a lower temperature for nanomodified CFRP.

In epoxy tensile specimens, the increase in polymer curing correlates to lower strain at failure, higher tensile strength, and higher Young's modulus. Larger differences in peak temperatures between oven cured and room temperature cured nanomodified CFRP variations correlates to smaller changes in tensile strength. However, the degree of curing does not correlate directly with the trends of CFRP specimens.

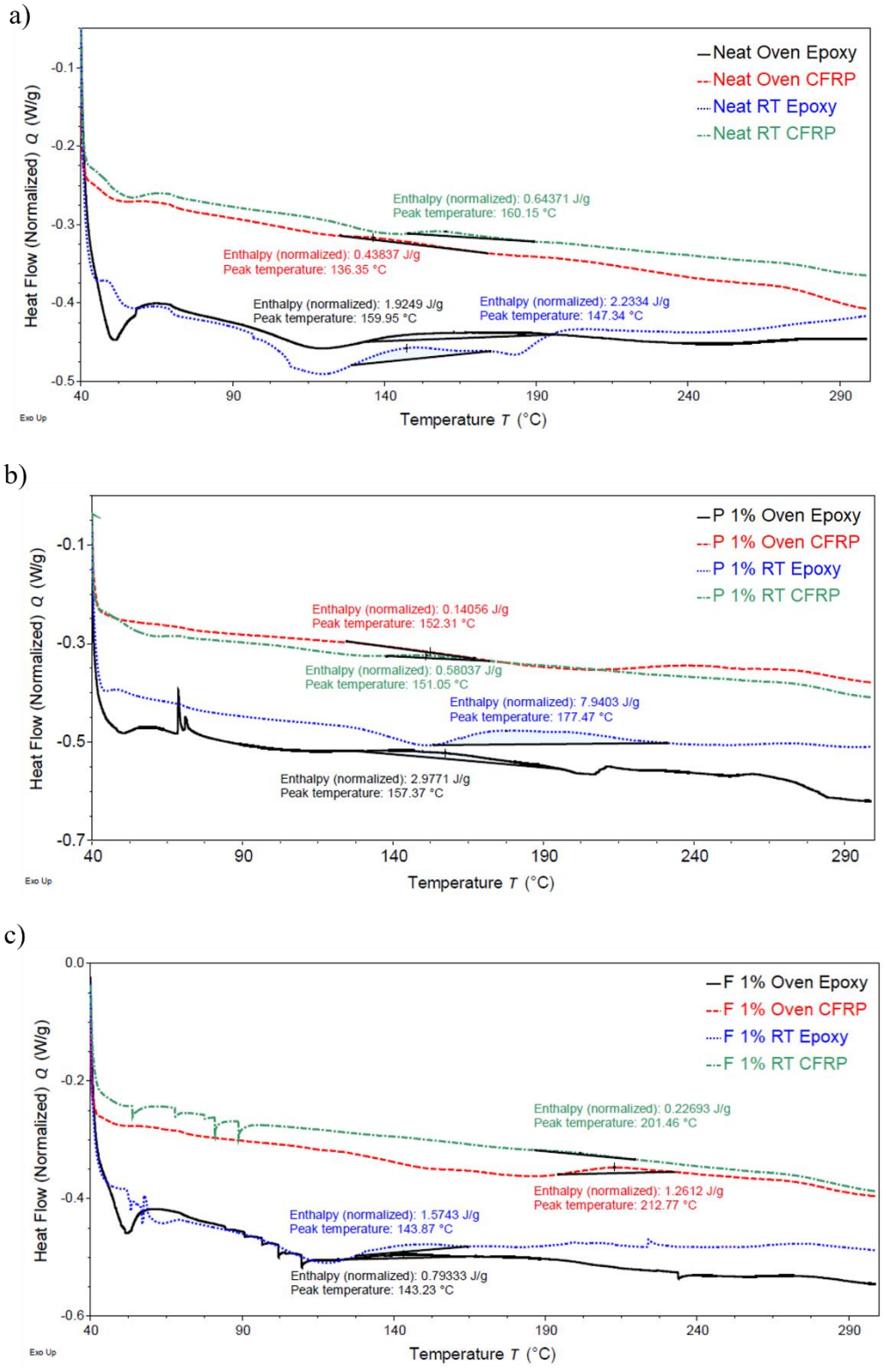

Figure 28: DSC curves for dynamic testing of (a) neat, (b)P 1%, (c) and F 1% epoxy and CFRP cured at room temperature (RT 30 ℃) and elevated temperature (Oven 110 ℃).

Table 13: DSC results for all cured epoxy and CFRP types cured at room temperature (RT, 30 ℃) and cured in the oven (110 ℃).

Specimen Type	**Normalized Enthalpy Ht (J/g)**	**Peak Temperature (℃)**
Neat Epoxy RT	2.2334	129.44
Neat Epoxy Oven	1.9249	133.61
Neat CFRP RT	0.6437	160.15
Neat CFRP Oven	0.4384	136.35
P 1% Epoxy RT	7.9403	177.47
P 1% Epoxy Oven	2.9771	157.37
P 1% CFRP RT	0.5804	151.05
P 1% CFRP Oven	0.1406	152.31
F 1% Epoxy RT	1.5743	143.87
F 1% Epoxy Oven	0.7933	143.23
F 1% CFRP RT	0.2269	201.46
F 1% CFRP Oven	1.2612	212.77

Chapter 5: Conclusions and Recommendations

5.1 Conclusions

The following conclusions can be drawn from the study results:

- Nanomodification decreased the tensile strength of all CFRP composites and epoxies when cured at room temperature (30 ℃).
- Compared to neat room temperature-cured CFRP, only nanomodification of CFRP with functionalized-COOH 1% MWCNTs increased tensile strength of CFRP composites when cured at 110 ℃.
- Nanomodification increased the tensile strength of all epoxies when cured at 110 ℃ compared to neat room temperature specimens.
- Nanomodification of epoxy with 1% pristine MWCNTs resulted in higher tensile strength than epoxy nanomodified with 1% functionalized-COOH MWCNTs.
- Nanomodification of CFRP with 1% functionalized-COOH MWCNTs resulted in higher tensile strength than CFRP nanomodified with 1% pristine MWCNTs.
- CFRP increased in interfacial adhesion strength when nanomodified and cured at either room temperature (30 ℃) or 110 ℃ but increased more with higher curing temperature.
- Interfacial adhesion strength of CFRP was similar for 1% pristine CNT and 1% functionalized-COOH CNT-modified CFRP cured at room temperature (30 ℃).
- Interfacial adhesion strength of 1% functionalized-COOH CFRP was higher than neat and 1% pristine CFRP cured at elevated temperature (110 ℃).

- All epoxies cured at room temperature exhibited lower tensile strength compared to epoxies cured at 110 ℃.
- All epoxies cured at room temperature exhibited higher ductility compared to epoxies cured at 110 ℃, which exhibited brittle behavior.
- CFRP mechanical behavior did not change as significantly as epoxy with different curing temperatures.
- For room temperature cured epoxies, incorporation of functionalized-COOH MWCNTs increased the degree of cure compared to neat epoxy.
- Immediate placement of epoxy into an elevated temperature environment for curing can improve the degree of curing for neat and nanomodified epoxies, indicated by lower enthalpy values in DSC testing.
- DSC results indicate the differences in polymer characteristics of epoxy and CFRP when cured at different temperatures and explain why there are differences in tensile behavior between the same epoxies cured at different temperatures.
- Curing temperature of CFRP can be adjusted to change mechanical and material behavior to achieve a desired behavior.

5.2 Future Work Recommendations

To further investigate the effect of curing environment on the mechanical and material properties of nanomodified FRP, the following work is recommended:

- Testing of short beam shear specimens of nanomodified epoxy cured at room temperature versus elevated temperature.

- Testing of different curing temperatures to enhance ability to achieve target metrics.
- Investigating the effect of nanomodification and curing temperature on different fiber and epoxy types with static tensile and peel testing.
- SEM imaging of epoxy samples cured at elevated temperature to compare microstructure.
- Investigating the effect of environmental effects on FRP composites.
- Improving the CNT dispersion quality in the epoxy matrix could improve mechanical performance of the CFRP. Adjustments in the dispersion procedure, as well as experimenting with different additives to the solution could be beneficial.
- Testing uncured epoxy resin with DSC to evaluate precise degree of cure.

References

Abdalla, M., D. Dean, P. Robinson and E. Nyairo (2008). "Cure behavior of epoxy/MWCNT nanocomposites: The effect of nanotube surface modification." Polymer **49**(15): 3310-3317.

Alkhrdaji, T. (2015) "Strengthening of Concrete Structures Using FRP Composites."

Allaoui, A. and N.-E. El Bounia (2009). "How carbon nanotubes affect the cure kinetics and glass transition temperature of their epoxy composites? – A review." Express Polymer Letters **3**(9): 588-594.

Bansal, S. A., V. Khanna, Twinkle, A. P. Singh and S. Kumar (2022). "Small percentage reinforcement of carbon nanotubes (CNTs) in epoxy(bisphenol-A) for enhanced mechanical performance." Materials Today: Proceedings **61**: 275-279.fe

Boroujeni, A. Y., M. Tehrani, A. J. Nelson and M. Al-Haik (2014). "Hybrid carbon nanotube–carbon fiber composites with improved in-plane mechanical properties." Composites Part B: Engineering **66**: 475-483.

Chakraborty, A. K., T. Plyhm, M. Barbezat, A. Necola and G. P. Terrasi (2011). "Carbon nanotube (CNT)–epoxy nanocomposites: a systematic investigation of CNT dispersion." Journal of Nanoparticle Research **13**(12): 6493-6506.

Chen, J. F. and J. G. Teng (2003). "Shear capacity of FRP-strengthened RC beams: FRP debonding." Construction and Building Materials **17**(1): 27-41.

Cividanes, L. S., W. Franceschi, F. V. Ferreira, B. R. C. Menezes, R. C. M. Sales and G. P. Thim (2017). "How Do CNT affect the branch and crosslink reactions in CNT-epoxy." Materials Research Express **4**(10): 105101.

Cividanes, L. S., E. A. N. Simonetti, M. B. Moraes, F. W. Fernandes and G. P. Thim (2014). "Influence of carbon nanotubes on epoxy resin cure reaction using different techniques: A comprehensive review." Polymer Engineering & Science **54**(11): 2461-2469.

Dodiuk, H. and S. H. Goodman (2022). Chapter 1 - Introduction. Handbook of Thermoset Plastics (Fourth Edition). H. Dodiuk. Boston, William Andrew Publishing**:** 1-11.

Eurofins Scientific. (2023). "Characterization of Polymers using Differential Scanning Calorimetry (DSC)." 2023, from https://www.eag.com/app-note/characterization-of-polymers-using-differential-scanning-calorimetry-dsc/.

Eyckens, D. J., J. D. Randall, F. Stojcevski, E. Sarlin, S. Palola, M. Kakkonen, C. Scheffler and L. C. Henderson (2020). "Examining interfacial interactions in a range of polymers using

poly(ethylene oxide) functionalized carbon fibers." Composites Part A: Applied Science and Manufacturing **138**: 106053.

Filchakova, M. (2021). "Single-walled carbon nanotubes: structure, properties, applications, and health & safety." Retrieved 11/20/22, 2022, from https://tuball.com/articles/single-walled-carbon-nanotubes.

Haley, J. S. (2011). Climatology of Freeze-Thaw Days in the Conterminous United States: 1982-2009. Master of Arts in Geography, Kent State University.

Hesami, M., R. Bagheri and M. Masoomi (2014). "Combination effects of carbon nanotubes, MMT and phosphorus flame retardant on fire and thermal resistance of fiber-reinforced epoxy composites." Iranian Polymer Journal **23**.

Irshidat, M. R. and M. H. Al-Saleh (2016). "Effect of using carbon nanotube modified epoxy on bond–slip behavior between concrete and FRP sheets." Construction and Building Materials **105**: 511-518.

Jain, R. and L. Lee (2012). Fiber Reinforced Polymer (FRP) Composites for Infrastructure Applications Focusing on Innovation, Technology Implementation and Sustainability / edited by Ravi Jain, Luke Lee, Dordrecht : Springer Netherlands : Imprint: Springer.

Jiang, F., X. Han, Y. Wang, P. Wang, T. Zhao and K. Zhang (2022). "Effect of freeze-thaw cycles on tensile properties of CFRP, bond behavior of CFRP-concrete, and flexural performance of CFRP-strengthened concrete beams." Cold Regions Science and Technology **194**: 103461.

Joshi, S. C. and V. Dikshit (2012). "Enhancing interlaminar fracture characteristics of woven CFRP prepreg composites through CNT dispersion." Journal of Composite Materials **46**(6): 665-675.

Khan, S. and J.-K. Kim (2011). "Impact and Delamination Failure of Multiscale Carbon Nanotube-Fiber Reinforced Polymer Composites: A Review." International Journal of Aeronautical and Space Sciences **12**.

Kodur, V., S. Venkatachari, V. A. Matsagar and S. B. Singh (2022). "Test Methods for Characterizing the Properties of Fiber-Reinforced Polymer Composites at Elevated Temperatures." Polymers (Basel) **14**(9).

Kosukegawa, H., Yamada, R., Tamonoki, S., Sato N., Ura, K., Takagi, T. (2018). Nondestructive Evaluation of Hardening Degree of Epoxy Resin in CFRP with Eddy Current Testing.

Li, B., W. Gong, X. Jing and B. Zheng (2021). "Effect of NaCl concentration on the dispersion, stability and rheological properties of MWNTs by CMC." Journal of Dispersion Science and Technology **42**(14): 2043-2052.

Li, C. and T.-W. Chou (2003). “Elastic moduli of multi-walled carbon nanotubes and the effect of van der Waals forces.” Composites Science and Technology **63**(11): 1517-1524.

Mansoor, M., M. Shahid and A. Habib (2014). “Strengthening of Bisphenol-A Epoxy Resin by the Addition of Multi-Wall Carbon Nanotubes.” Arabian Journal for Science and Engineering **39**(8): 6411-6420.

Ng, H. M., N. M. Saidi, F. S. Omar, K. Ramesh, S. Ramesh and S. Bashir (2018). Thermogravimetric Analysis of Polymers. Encyclopedia of Polymer Science and Technology**:** 1-29.

Polymer Science Learning Center. (2023). “The Glass Transition.”

Postek, M. T. and A. E. Vladár (2013). “Does your SEM Really tell the truth?—how would you know? Part 1.” Scanning **35**(6): 355-361.

Qiao, L. and K. Du (2022). “Scalable production of high-quality carbon nanotube dispersion in aqueous solution using cellulose as dispersant by a freezing/thawing process.” Journal of Colloid and Interface Science **623**: 1200-1209.

Rajendran, D., R. Ramalingame, A. Adiraju, H. Nouri and O. Kanoun (2022). “Role of Solvent Polarity on Dispersion Quality and Stability of Functionalized Carbon Nanotubes.” Journal of Composites Science **6**(1): 26.

Robiul Islam, R., A. Md. Hasan, J. Md. Abu and A. Md. Mahmodul (2019). “Carbon nanotubes agglomeration in reinforced composites: A review.” AIMS Materials Science **6**(5): 756-780.

Singh, S. B., S. Vummadisetti and H. Chawla (2018). “Influence of curing on the mechanical performance of FRP laminates.” Journal of Building Engineering **16**: 1-19.

Soliman, E., M. Al-Haik and M. Reda Taha (2012). “On and off-axis tension behavior of fiber reinforced polymer composites incorporating multi-walled carbon nanotubes.” Journal of Composite Materials - J COMPOS MATER **46**: 1661-1675.

Uddin, N. (2013). Developments in fiber-reinforced polymer (FRP) composites for civil engineering, Cambridge, UK : Woodhead Publishing Limited.

Zhang, W., X. Deng, G. Sui and X. Yang (2019). “Improving interfacial and mechanical properties of carbon nanotube-sized carbon fiber/epoxy composites.” Carbon **145**: 629-639.

Zhou, T., X. Wang, H.-g. Zhu and T. Wang (2009). “Influence of carboxylic functionalization of MWCNTs on the thermal properties of MWCNTs/DGEBA/EMI-2,4 nanocomposites.” Composites Part A-applied Science and Manufacturing **40**: 1792-1797.

Appendix A: Effect of Freeze-Thaw on Nanomodified Fiber-Reinforced Polymers

Introduction to Freeze-thaw

As infrastructure ages, FRP has been successfully implemented in repair and strengthening of deteriorating buildings and bridges. However, there is still little research on how the harsh environmental conditions that structures must endure affect this material, and many of the studies that do exist present contradictory results or are inconclusive (Jiang et al. 2022). One potentially harsh condition is the natural phenomenon of freeze-thaw, which entails the cyclic freezing and thawing of water within a material's pores. In the United States, some states see up to 250 freeze-thaw cycles annually, and the expansive stress caused by the freezing water can be as large as 250 MPa, causing irreversible damage to the material (Haley 2011, Qiao et al. 2022). Therefore, as a common and potentially damaging occurrence, freeze-thaw effects on exposed construction materials need to be investigated and documented to determine more accurate service lives for FRP to be used in design. Over time, freeze-thaw cycles gradually damage the bond interface between the FRP and the strengthened material, leading to debonding failure before the full strength of the FRP is utilized (Jiang et al. 2022). To understand and prevent this debonding failure, further investigation of freeze-thaw impact and methods of bond preservation are necessary.

In this project, protective measures to prevent damage from freeze-thaw were explored. By exploring the response of FRP composites nanomodified with several types and concentrations of CNTs exposed to freeze-thaw conditions, the effect of this harsh environmental phenomenon can be better understood, and steps can be made to improve FRP composites for use in durable and

lasting infrastructure. As the expansive forces during freezing push the layers of FRP apart and cause failure along composite planes or matrix cracking, CNTs hold them together, bridging the gaps across cracks and improving bond strengths (Li et al. 2021). With the addition of CNTs to the FRP used to reinforce structures, material deterioration from harsh environmental conditions could be significantly reduced.

Methods and Materials

Testing Overview

Seven types of CFRP plates were cast with the VAHT procedure described in section 3.3: neat, nanomodified with pristine CNTs (0.5%, 1.0%, and 1.5% by weight pristine nanotubes), and nanomodified with functionalized CNTs (0.5%, 1.0%, 1.5% wt. functionalized-COOH nanotubes). This matrix is outlined in Figure 29. For 0, 50, 100, 150, 200, and 250 freeze-thaw cycles, ten CFRP tensile specimens of each CNT type were made according to section 3.5. CFRP tensile specimens were placed in an environmental chamber submerged in water for 250 freeze-thaw cycles. For every 50 cycles, one set of ten specimens was removed from the chamber and evaluated through a series of destructive tensile testing per section 3.5. The tabs were adhered to the tensile specimens after removal from the environmental chamber and drying at room temperature for 24 hours.

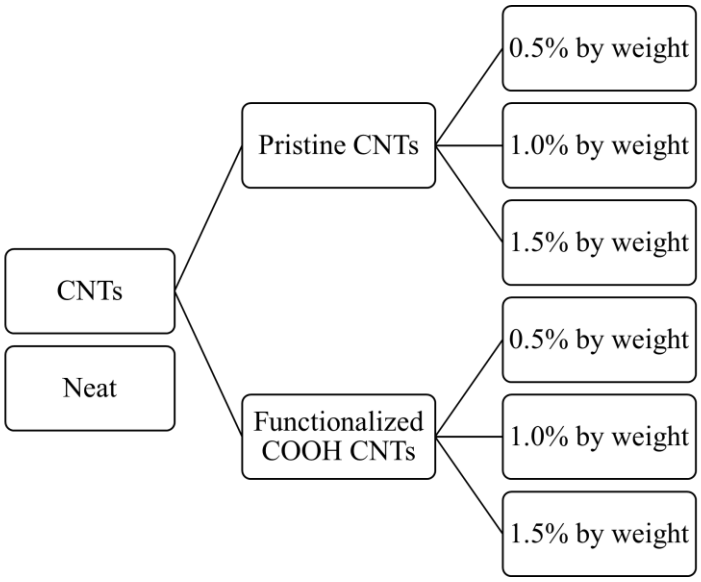

Figure 29: Matrix of CFRP types manufactured for freeze-thaw cycling.

Freeze-thaw Cycling

Ten CFRP tensile specimens of each type of chosen nanotube and cycle designation were submerged in water inside an environmental chamber. The freeze-thaw chamber freeze phase occurred at 0 °C, and the thawing occurred at 40 °C. Thermocouples were placed inside the controlled operation of the chamber to most accurately measure the temperature of the specimens in the chamber and ensure complete freeze-thaw cycles. Specimens were removed approximately every 50 cycles up to 250 cycles. After removal from the environmental chamber, specimens were left at room temperature to dry for 24 hours before adhering tabs.

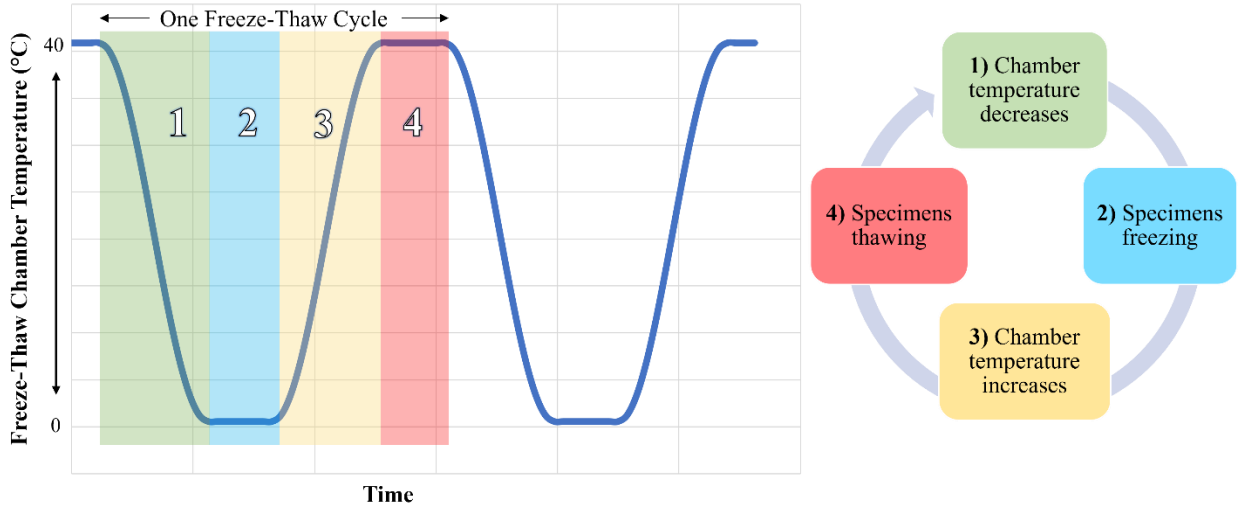

Figure 30: Freeze-thaw cycling in environmental chamber.

Mechanical Testing

The static tensile testing procedure described in section 3.5 was followed for all CFRP specimens. Off-axis loading was implemented to enhance the differences between nanomodified matrices.

Results and Analysis

Results of tensile testing reveal the evolution of mechanical behavior of the CFRP over 250 freeze-thaw cycles with a 79% confidence level. Representative failure mode for all CFRP specimens is shown in Figure 19. Shown in Figure 31(a), neat and functionalized-COOH 1% wt. CFRP had higher average tensile strengths compared to other nanomodified CFRP. While the neat CFRP displayed a steady drop in tensile strength with the increase in freeze-thaw cycles, functionalized-COOH 1% wt. CFRP tensile strength increased with the number of cycles.

Additionally, the strength of nanomodified variations does not drop permanently like the neat CFRP that dropped by just over 13 MPa. As seen in Figure 31(b), functionalized-COOH 1% CFRP consistently has significantly higher strain compared to all other CFRP types. Shown in Figure 31(c), neat CFRP has the higher Young's modulus of all types, likely due to the elastic nature of CNTs. While plain epoxy is brittle, CNTs are inherently springy and have a high modulus of elasticity (Li et al. 2003). The low tensile strength of the CFRP plates with 0.5% wt. compared to 1% wt. may have been due to the low concentration of CNTs in the epoxy that may not have been enough to make a difference in interlaminar engagement. Similarly, FRP with a CNT concentration that is too high (1.5% wt.) may experience more CNT agglomeration in the epoxy, not allowing the CNTs to bond properly to the matrix.

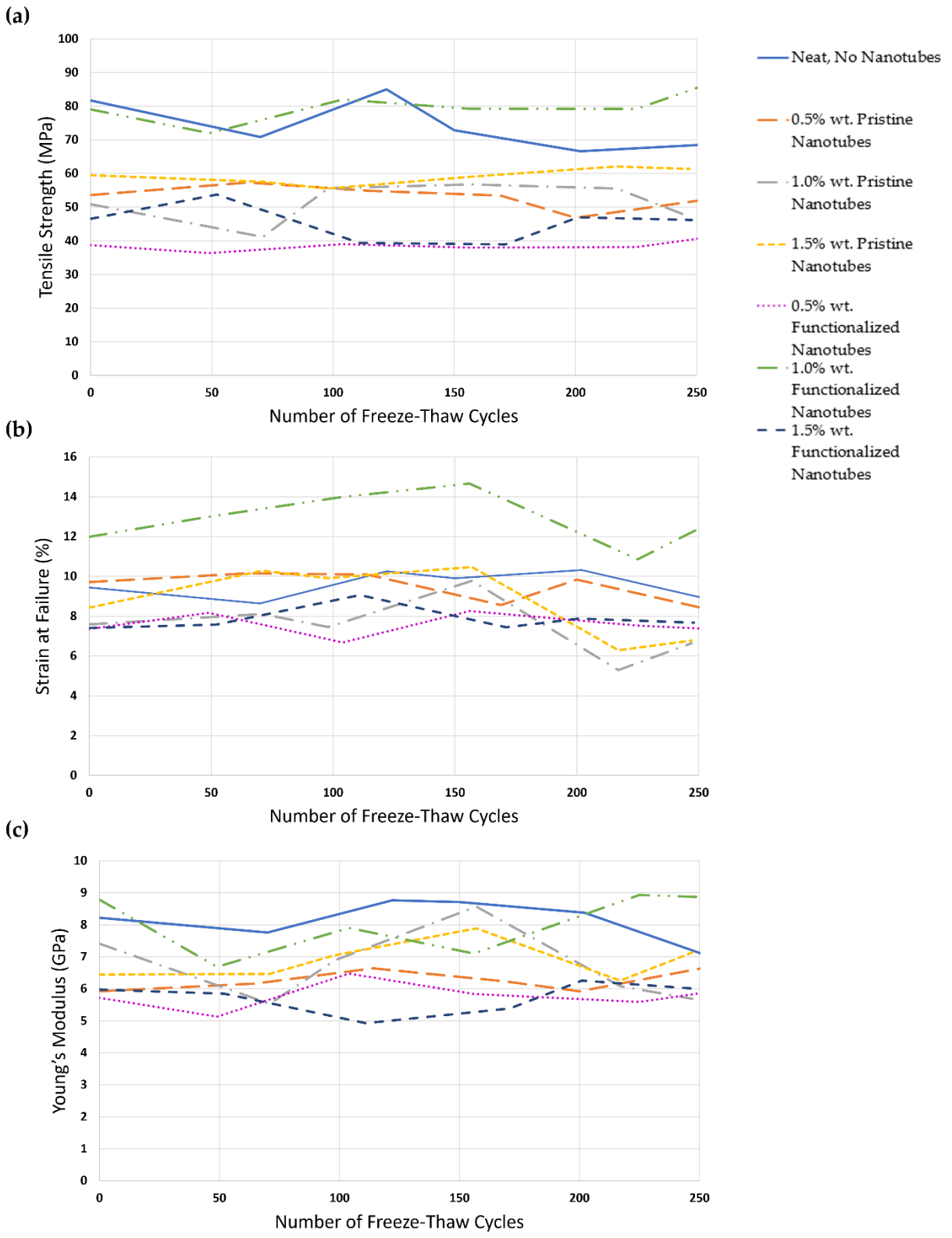

Figure 31: Evolution of (a) strength, (b) strain, and (c) modulus of elasticity of CFRP tensile specimens over 250 freeze-thaw cycles.

Median stress-strain behavior at 0 and 250 freeze-thaw cycles can be seen in Figure 32. Specimens display yielding behavior, unlike typical brittle linear elastic behavior seen in CFRP loaded on-axis. Enhanced performance of the functionalized-COOH 1% CFRP specimens is attributed to the ability of carboxyl-functionalized CNTs to bond better with epoxy matrix (Zhang et al. 2019).

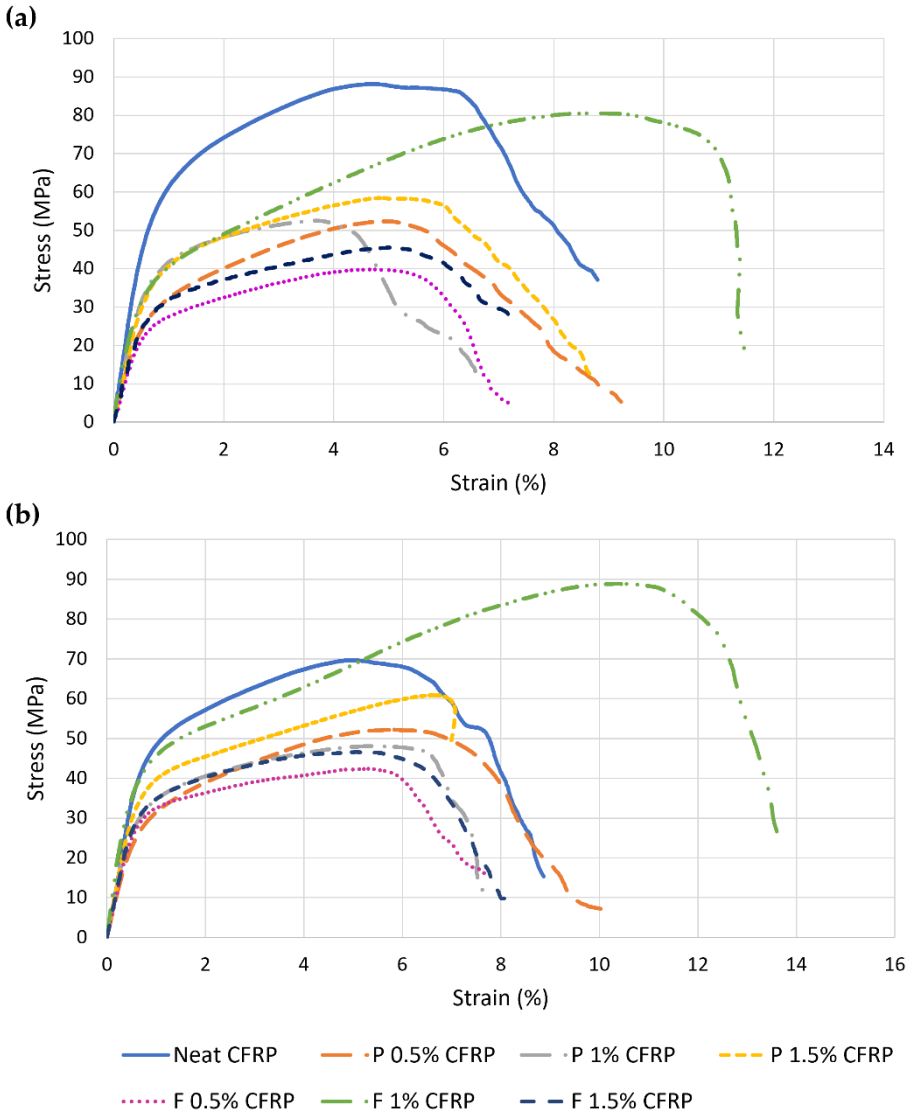

Figure 32: Stress-strain relationship for CFRP after (a) 0 freeze-thaw cycles and (b) 250 freeze-thaw cycles.

Conclusions for Freeze-thaw Study

The following conclusions can be drawn from the freeze-thaw study results:

- The tensile strength of neat CFRP was higher than that of all nanomodified CFRP at 0 freeze-thaw cycles.
- The tensile strength of functionalized-COOH 1% wt. CFRP increased with the number of freeze-thaw cycles, surpassing the strength of neat CFRP.
- After 250 freeze-thaw cycles, functionalized-COOH 1% wt. CFRP had the highest tensile strength, strain at failure, and Young's modulus.
- The weight concentration of MWCNTs significantly impacts the mechanical properties of CFRP and changes how mechanical properties evolve with freeze-thaw exposure.
- The failure behavior of nanomodified and neat CFRP exposed to 250 freeze-thaw cycles did not change.
- Utilization of functionalized-COOH MWCNTs with a 1% wt. concentration in CFRP may prevent the degradation of mechanical properties of CFRP and even enhance them.

Future Work with Freeze-thaw

To further investigate the effect of freeze-thaw cycling on the mechanical and material properties of nanomodified FRP, the following work is recommended:

- Tensile testing of isolated nanomodified epoxy matrix over 250 freeze-thaw cycles.
- Tensile testing of nanomodified CFRP exposed to over 250 freeze-thaw cycles to investigate extent of freeze-thaw durability.

- Tensile testing of nanomodified CFRP cured at room temperature (30 ℃) and 110 ℃ exposed to 250 freeze-thaw cycles to evaluate effect of curing temperature on freeze-thaw durability.
- Short beam shear testing of nanomodified epoxy to evaluate interlaminar shear property changes with exposure to freeze-thaw cycles.
- Peel testing of CFRP exposed to 250 freeze-thaw cycles to evaluate the effect of freeze-thaw on interfacial adhesion strength.
- Material testing of epoxy before and after 250 freeze-thaw cycles to identify chemical/bond changes within the polymer structure.

References for Freeze-thaw Study

Haley, J. S. (2011). Climatology of Freeze-Thaw Days in the Conterminous United States: 1982-2009. Master of Arts in Geography, Kent State University.

Jiang, F., X. Han, Y. Wang, P. Wang, T. Zhao and K. Zhang (2022). "Effect of freeze-thaw cycles on tensile properties of CFRP, bond behavior of CFRP-concrete, and flexural performance of CFRP-strengthened concrete beams." Cold Regions Science and Technology **194**: 103461.

Li, B., W. Gong, X. Jing and B. Zheng (2021). "Effect of NaCl concentration on the dispersion, stability and rheological properties of MWNTs by CMC." Journal of Dispersion Science and Technology **42**(14): 2043-2052.

Li, C. and T.-W. Chou (2003). "Elastic moduli of multi-walled carbon nanotubes and the effect of van der Waals forces." Composites Science and Technology **63**(11): 1517-1524.

Qiao, L. and K. Du (2022). "Scalable production of high-quality carbon nanotube dispersion in aqueous solution using cellulose as dispersant by a freezing/thawing process." Journal of Colloid and Interface Science **623**: 1200-1209.

Zhang, W., X. Deng, G. Sui and X. Yang (2019). "Improving interfacial and mechanical properties of carbon nanotube-sized carbon fiber/epoxy composites." Carbon **145**: 629-639.

Appendix B: Data from CFRP Tensile Testing over Freeze-thaw Cycling

Table 14: Results from tensile testing of CFRP after zero freeze-thaw cycles.

		Tensile Strength (MPa)	**Strain (%)**	**Modulus of Elasticity (GPa)**
Neat	Mean	81.72	9.44	8.22
	Standard Deviation	4.27	1.15	0.8524
	COV (%)	5.23	12.22	10.38
P 0.5%	Mean (%)	53.57 (-34%)*	9.72 (3%)*	5.92 (-28%)*
	Standard Deviation	4.66	0.56	0.60
	COV (%)	8.70	5.77	10.14
P 1.0%	Mean (%)	50.88 (-38%)*	7.58 (-20%)*	7.41 (-10%)*
	Standard Deviation	3.4529	1.13	0.78
	COV (%)	0.0679	14.93	10.47
P 1.5%	Mean (%)	59.45 (-27%)*	8.43 (-11%)*	6.44 (-22%)*
	Standard Deviation	3.67	0.94	0.38
	COV (%)	6.18	11.10	5.83
F 0.5%	Mean (%)	38.75 (-53%)*	7.36 (-22%)*	5.72 (-31%)*
	Standard Deviation	1.67	0.24	0.44
	COV (%)	4.31	3.23	7.69
F 1.0%	Mean (%)	79.03 (-3%)*	11.99 (27%)*	8.79 (7%)*
	Standard Deviation	2.51	1.39	1.27
	COV (%)	3.18	11.58	14.46
F 1.5%	Mean (%)	46.54 (-43%)*	7.40 (-22%)*	5.98 (-27%)*
	Standard Deviation	4.00	0.82	1.34
	COV (%)	8.60	11.06	22.36

*Compared to neat CFRP for zero freeze-thaw cycles

Table 15: Results from tensile testing of CFRP after 50 freeze-thaw cycles.

		Tensile Strength (MPa)	**Strain (%)**	**Modulus of Elasticity (GPa)**
Neat	Mean	70.86 (-13%)*	8.64 (-8%)*	7.76 (-6%)*
	Standard Deviation	4.55	1.03	0.98
	COV (%)	6.43	11.94	12.67
P 0.5%	Mean (%)	57.30 (-30%)*	10.16 (8%)*	6.16 (-25%)*
	Standard Deviation	2.13	0.66	0.83
	COV (%)	3.71	6.49	13.40
P 1.0%	Mean (%)	41.16 (-50%)*	8.11 (-14%)*	5.53 (-33%)*
	Standard Deviation	2.68	0.48	0.68
	COV (%)	6.52	5.92	12.24
P 1.5%	Mean (%)	57.57 (-30%)*	10.28 (9%)*	6.46 (-21%)*
	Standard Deviation	4.67	0.67	0.80
	COV (%)	8.11	6.51	12.42
F 0.5%	Mean (%)	36.32 (-56%)*	8.18 (-13%)*	5.13 (-38%)*
	Standard Deviation	0.77	0.84	0.56
	COV (%)	2.12	10.23	10.88
F 1.0%	Mean (%)	72.00 (-12%)*	13.00 (38%)*	6.69 (-19%)*
	Standard Deviation	3.14	1.31	0.98
	COV (%)	4.36	10.08	14.69
F 1.5%	Mean (%)	53.77 (-34%)*	7.58 (-20%)*	5.85 (-29%)*
	Standard Deviation	3.50	0.36	0.87
	COV (%)	6.50	4.75	14.85

*Compared to neat CFRP for zero freeze-thaw cycles

Table 16: Results from tensile testing of CFRP after 100 freeze-thaw cycles.

		Tensile Strength (MPa)	**Strain (%)**	**Modulus of Elasticity (GPa)**
Neat	Mean	84.99 (4%)*	10.26 (9%)*	8.76 (7%)*
	Standard Deviation	3.83	0.45	0.78
	COV (%)	4.50	4.39	8.88
P 0.5%	Mean (%)	54.88 (-33%)*	10.09 (7%)*	6.64 (-19%)*
	Standard Deviation	1.99	0.43	0.57
	COV (%)	3.63	4.27	8.52
P 1.0%	Mean (%)	55.61 (-32%)*	7.45 (-21%)*	6.89 (-16%)*
	Standard Deviation	6.16	1.45	0.45
	COV (%)	11.08	19.43	6.47
P 1.5%	Mean (%)	55.54 (-32%)*	9.91 (5%)*	7.05 (-14%)*
	Standard Deviation	2.66	1.28	0.84
	COV (%)	4.79	12.96	11.90
F 0.5%	Mean (%)	38.99 (-52%)*	6.68 (-29%)*	6.47 (-21%)*
	Standard Deviation	3.01	0.79	0.60
	COV (%)	7.72	11.78	9.22
F 1.0%	Mean (%)	82.01 (0.36%)*	13.99 (48%)*	7.90 (-4%)*
	Standard Deviation	5.20	1.41	0.42
	COV (%)	6.34	10.09	5.37
F 1.5%	Mean (%)	39.33 (-52%)*	9.06 (-4%)*	4.93 (-40%)*
	Standard Deviation	1.43	0.80	0.86
	COV (%)	3.64	8.85	17.43

*Compared to neat CFRP for zero freeze-thaw cycles

Table 17: Results from tensile testing of CFRP after 150 freeze-thaw cycles.

		Tensile Strength (MPa)	**Strain (%)**	**Modulus of Elasticity (GPa)**
Neat	Mean	72.89 (-11%)*	9.90 (5%)*	8.71 (6%)*
	Standard Deviation	3.45	0.43	1.85
	COV (%)	4.74	4.38	21.19
P 0.5%	Mean (%)	53.48 (-35%)*	8.56 (-9%)*	6.23 (-24%)*
	Standard Deviation	2.07	1.18	0.59
	COV (%)	3.86	13.83	9.53
P 1.0%	Mean (%)	56.74 (-31%)*	9.78 (4%)*	8.57 (4%)*
	Standard Deviation	3.74	1.00	3.65
	COV (%)	6.58	10.22	42.57
P 1.5%	Mean (%)	59.09 (-28%)*	10.47 (11%)*	7.89 (-4%)*
	Standard Deviation	4.36	1.32	0.97
	COV (%)	7.37	12.56	12.32
F 0.5%	Mean (%)	38.03 (-53%)*	8.25 (-13%)*	5.84 (-29%)*
	Standard Deviation	1.85	0.45	0.47
	COV (%)	4.86	5.49	8.01
F 1.0%	Mean (%)	79.27 (-3%)*	14.67 (55%)*	7.10 (-14%)*
	Standard Deviation	5.71	1.49	1.29
	COV (%)	7.20	10.19	18.23
F 1.5%	Mean (%)	38.95 (-52%)*	7.44 (-21%)*	5.39 (-34%)*
	Standard Deviation	2.80	0.92	0.40
	COV (%)	7.19	12.40	7.38

*Compared to neat CFRP for zero freeze-thaw cycles

Table 18: Results from tensile testing of CFRP after 200 freeze-thaw cycles.

		Tensile Strength (MPa)	**Strain (%)**	**Modulus of Elasticity (GPa)**
Neat	Mean	66.58 (-19%)*	10.32 (9%)*	8.38 (2%)*
	Standard Deviation	1.05	0.46	0.86
	COV (%)	1.57	4.49	10.29
P 0.5%	Mean (%)	46.82 (-43%)*	9.84 (-4%)*	5.92 (-28%)*
	Standard Deviation	2.20	0.56	2.33
	COV (%)	4.69	5.66	39.29
P 1.0%	Mean (%)	55.55 (-32%)*	5.30 (-44%)*	6.08 (-26%)*
	Standard Deviation	1.07	0.31	0.23
	COV (%)	1.93	5.88	3.81
P 1.5%	Mean (%)	62.08 (-24%)*	6.30 (-33%)*	6.26 (-24%)*
	Standard Deviation	3.15	0.54	0.89
	COV (%)	5.07	8.57	14.21
F 0.5%	Mean (%)	38.11 (-53%)*	7.52 (-20%)*	5.59 (-32%)*
	Standard Deviation	2.12	0.73	0.40
	COV (%)	5.57	9.67	7.11
F 1.0%	Mean (%)	79.15 (-3%)*	10.86 (15%)*	8.93 (9%)*
	Standard Deviation	6.68	1.06	1.42
	COV (%)	8.44	9.78	15.92
F 1.5%	Mean (%)	46.99 (-42%)*	7.89 (-16%)*	6.25 (-24%)*
	Standard Deviation	2.19	0.37	0.42
	COV (%)	4.65	4.66	6.74

*Compared to neat CFRP for zero freeze-thaw cycles

Table 19: Results from tensile testing of CFRP after 250 freeze-thaw cycles.

		Tensile Strength (MPa)	**Strain (%)**	**Modulus of Elasticity (GPa)**
Neat	Mean	69.25 (-15%)*	8.37 (-11%)*	6.57 (-20%)*
	Standard Deviation	2.54	0.92	0.64
	COV (%)	3.67	10.96	9.77
P 0.5%	Mean (%)	52.86 (-35%)*	8.18 (-13%)*	6.77 (-18%)*
	Standard Deviation	4.39	0.68	0.70
	COV (%)	8.31	8.27	10.40
P 1.0%	Mean (%)	47.20 (-42%)*	6.64 (-30%)*	5.69 (-31%)*
	Standard Deviation	3.15	0.71	0.92
	COV (%)	6.68	10.66	16.12
P 1.5%	Mean (%)	61.38 (-25%)*	6.77 (-28%)*	7.13 (-13%)*
	Standard Deviation	5.26	0.30	0.87
	COV (%)	8.56	4.37	12.22
F 0.5%	Mean (%)	42.25 (-48%)*	7.28 (-23%)*	6.05 (-26%)*
	Standard Deviation	2.63	0.50	0.51
	COV (%)	6.23	6.94	8.41
F 1.0%	Mean (%)	89.67 (10%)*	13.43 (42%)*	8.83 (7%)*
	Standard Deviation	5.51	0.83	0.69
	COV (%)	6.14	6.14	7.87
F 1.5%	Mean (%)	46.20 (-43%)*	7.67 (-19%)*	6.01 (-27%)*
	Standard Deviation	1.56	0.32	0.94
	COV (%)	3.37	4.11	15.64

*Compared to neat CFRP for zero freeze-thaw cycles